International Journal of Advanced Pharmaceutical Sciences and Research (IJAPSR)
ISSN: 2582-7618 (Online), Volume-4 Issue-6, October 2024

Conductive Nanocomposites Based on Graphene and Natural Polymers

Nasser Thallaj

Abstract: ***This thesis focuses on the development of conductive nanocomposite materials based on graphene and natural polymers such as cellulose and chitosan. Graphene, a single layer of carbon atoms arranged in a honeycomb lattice, exhibits exceptional electrical, mechanical, and thermal properties, making it an attractive filler for polymer composites. However, the challenge lies in effectively dispersing graphene sheets within polymer matrices. The work presented explores new strategies for grafting polysaccharide chains onto oxidized graphite (graphene oxide) to improve its compatibility and dispersion in cellulose and chitosan matrices. The resulting composites were doped with gold or nickel nanoparticles to further enhance their electrical and catalytic properties. Detailed characterization techniques, including spectroscopic and microscopic methods, were employed to analyze the structure, morphology, and properties of the developed nanocomposites. The thesis is organized into three main parts: 1) a literature review on graphene, polysaccharides, and their biocomposites; 2) a description of the experimental materials and methods; and 3) a scientific discussion of the results, presented in the form of three research publications. The findings demonstrate the successful synthesis of conductive nanocomposites with improved compatibility and performance, opening up new avenues for the application of these sustainable and multifunctional materials in areas such as electronics, catalysis, and electromagnetic shielding.***

Keywords: Conductive nanocomposites; Graphene; Natural Polymers (Cellulose and Chitosan); Polysaccharide Grafting; Gold Nanoparticles; Nickel Nanoparticles; Electrical Properties; Catalytic Properties.

I. INTRODUCTION

The development of conductive nanocomposite materials has garnered significant attention in various fields, ranging from electronics to catalysis and electromagnetic shielding. This thesis focuses on the synthesis and characterization of innovative conductive nanocomposites based on graphene and natural polymers, specifically cellulose and chitosan. Graphene, a single-layer of carbon atoms arranged in a honeycomb lattice, exhibits exceptional electrical, mechanical, and thermal properties, making it an attractive filler for polymer composites. However, the challenge lies in effectively dispersing graphene sheets within polymer matrices to harness its full potential.

Manuscript received on 06 September 2024 | Revised Manuscript received on 22 September 2024 | Manuscript Accepted on 15 October 2024 | Manuscript published on 30 October 2024.

* Correspondence Author (s)
Prof. Dr. Nasser Thallaj*, Department of Pharmaceutical Chemistry and Drug Quality Control, Faculty of Pharmacy, Al-Rachid Privet University, Damascus (Syria), West Asia. Email ID: profthallaj@gmail.com ORCID ID: 0000-0002-6279-768X

This work explores new strategies for grafting polysaccharide chains onto oxidized graphite (graphene oxide) to improve its compatibility and dispersion in cellulose and chitosan matrices [1].

The resulting nanocomposites were further enhanced by doping with gold or nickel nanoparticles, which improved their electrical and catalytic properties. Detailed characterization techniques, including spectroscopic and microscopic methods, were employed to analyze the structure, morphology, and properties of the developed nanocomposites [2].

The findings of this work demonstrate the successful synthesis of conductive nanocomposites with improved compatibility and performance, opening up new avenues for the application of these sustainable and multifunctional materials [3]. The integration of graphene and natural polymers, coupled with the incorporation of metal nanoparticles, holds the potential to address the challenges faced in the fields of electronics, catalysis, and electromagnetic shielding [4]. By leveraging the unique properties of these materials, the research presented in this thesis contributes to the development of advanced functional materials that can meet the growing demands for versatile, environmentally-friendly, and high-performance solutions.

A. Synthesis and Functionalization of Graphene and its Derivatives

i. Graphite

Graphite is the most stable form of pure carbon at room temperature and pressure, and its structure has been identified [5]. Therefore, it is the most common form found, often occurring in coal. Graphite is a mineral species with a lamellar structure, where the planes are spaced 3.35 Å apart and consist of a hexagonal network of carbon atoms arranged in a honeycomb pattern (see Figure 1).

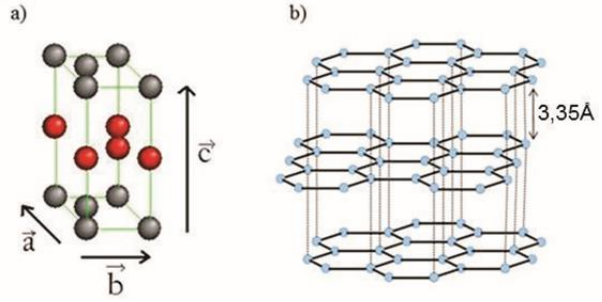

Figure 1: (A) Hexagonal Mesh and (B) Lamellar Structure of Graphite

The bonds within the planes of graphite are covalent, while the interplanar bonds are of the Van der Waals type, which are weak bonds [6].

This characteristic makes it easy for graphite to shed layers. Carbon has a tetravalent structure, and in its hexagonal arrangement, it is covalently bonded to only three neighboring atoms. The fourth valence electron forms weakly localized π bonds with neighbors in the same plane. This electron can participate in the electrical conduction of graphite, primarily within a single plane. An isolated sheet of graphite is known as "graphene." Other graphite-derived materials, such as expanded graphite and graphite nanowafers, are also marketed.

An isolated sheet of graphite is called "graphene." Other graphite-derived materials, such as expanded graphite and graphite nanowafers, are also marketed.

ii. Graphite Nanowafers

Graphite nanowafers (GNPs) are a finer form of nanocharges derived from natural graphite, measuring approximately 10 nm in thickness. The preparation of GNPs can be carried out either by the thermal expansion of graphite intercalated with chloride trifluoride [7], or by microwave irradiation of graphite intercalated with sulfuric acid, followed by ultrasonic spraying or ball milling [8]. GNPs can achieve diameters ranging from 1 to 15 µm, depending on the ultrasonic processing time [9]. The diameter can be further reduced to 1 nm by using a vibrating mill [9,10]. GNPs retain some oxygenated functional groups on the surface of their structure, which makes them slightly polar.

II. GRAPHENE

Graphene nanosheets were isolated for the first time in 2004, successfully obtaining a single graphene layer through the micromechanical cleavage of graphite, known as the "scotch tape" method [11,12]. Graphene is considered a perfect 2D material and has garnered significant interest in the scientific community for several years (see Figure 2).

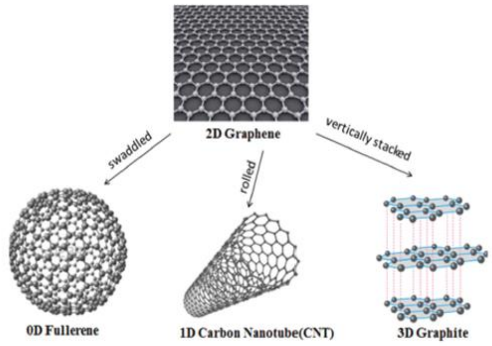

Figure 2: From Graphite to Graphene

Graphene, the material described in the previous paragraph, possesses a remarkable set of properties that make it exceptional. It consists of a single layer of carbon atoms arranged in a hexagonal lattice, with a thickness of approximately 70 picometers—just one millionth the width of a human hair [13]. This makes it the thinnest and lightest known material, weighing only 0.77 milligrams per square meter.

Graphene is also incredibly strong, with a Young's modulus close to 1000 GPa and a fracture limit of 130 GPa, making it one of the strongest materials ever discovered [14]. Its modulus of elasticity is around 0.25 TPa, which is extremely high [15].

In addition to its impressive mechanical properties, graphene has remarkable thermal conductivity, estimated at around 5,000 W/(m·K)—more than ten times higher than that of copper [16]. Theoretically, it could have a specific surface area of up to 2,630 m²/g [17]. Furthermore, graphene is impermeable to standard gases such as helium [18]. Electrically, graphene is an excellent conductor, with a conductivity of approximately 2,000,000 cm²/(V·s) or 200 S/m [19]. It can also withstand temperatures exceeding 3,000 degrees Celsius before melting [20].

In summary, the exceptional properties of graphene—ranging from its atomic-scale thickness to its unparalleled strength, conductivity, and thermal performance—explain the high expectations and intense research interest surrounding this remarkable material.

A. Main Routes of Obtaining

Currently, two main methods are used for the production of graphene at the scale of individual sheets: the "Bottom-up" method, which involves the growth of the sheet supported on a substrate, and the "Top-Down" method, which involves the formation of graphene powder. (See Figure 3.) [21].

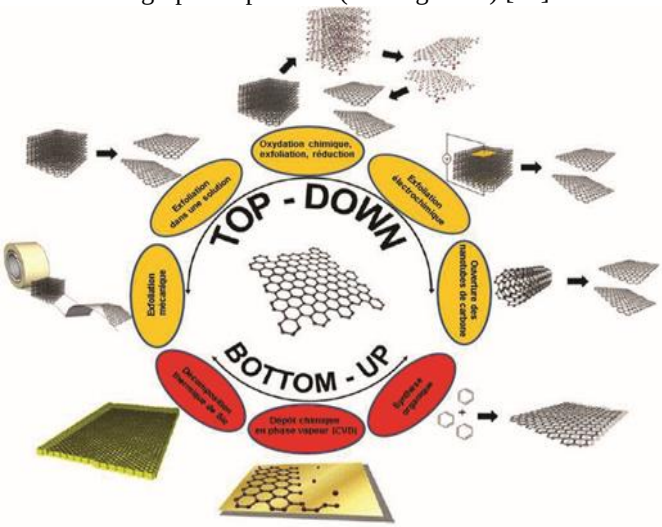

Figure 3: Different Ways of Obtaining Graphene

Among the most widely used graphene production techniques are micromechanical cleavage [12], chemical vapor deposition (CVD) [22,23], epitaxial growth on a SiC substrate [24,25], opening of carbon nanotubes [26,27], and reduction of oxidized graphite sheets [28]. In this section, we will describe the four main methods that appear in the literature.

i. Obtaining Graphene by Mechanical Exfoliation

This method is based on the Top-Down approach, where graphene nanosheets can be produced by direct exfoliation of graphite or oxidized graphite [29]. The technique known as graphite tape exfoliation, or graphite micromechanical cleavage, was the first experimental method used for the production of graphene nanoflakes (see Figure 4).

Retrieval Number: 100.1/ijapsr.F405404061024
DOI: 10.54105/ijapsr.F4054.04061024
Journal Website: www.ijapsr.latticescipub.com

Published By:
Lattice Science Publication (LSP)

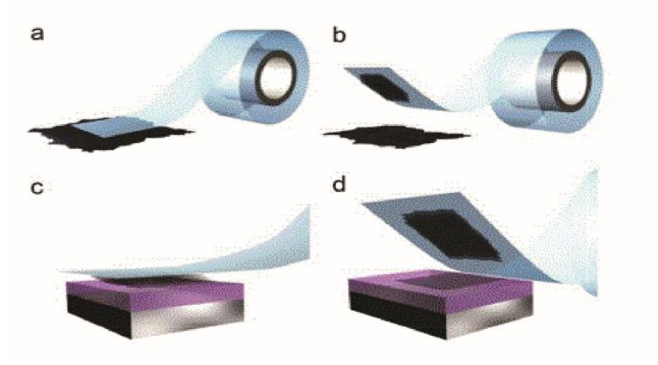

Figure 4: A-D) The steps of Graphene Synthesis from the Exfoliation of Graphite with Scotch

This discovery was made by Novoselov et al. in 2004. While this approach is very effective in obtaining nanosheets with excellent crystallinity, its extremely low yield makes large-scale industrial production unfeasible.

ii. Synthesis of Graphene by Chemical Vapor Deposition (CVD)

This method involves creating a graphene layer through chemical vapor deposition (CVD) on a metal substrate. Various metals are used for this process, including cobalt (Co), platinum (Pt), nickel (Ni), and copper (Cu).

The gaseous sources typically employed for this type of deposition are hydrocarbons such as methane, acetylene, or ethylene, which decompose upon contact with the metal surface to form graphene layers. Figure 5 illustrates the formation of graphene by CVD from a drop of gallium (Ga) placed on a tungsten (W) substrate [28-33].

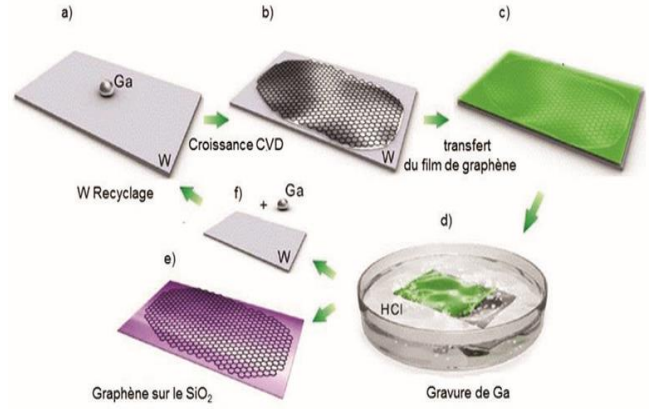

Figure 5: Different steps of graphene growth on a drop of Galium (Ga) supported on a substrate (W): a) a drop of Ga placed on a support sheet (W), b) CVD growth of graphene on the surface of the liquid Ga, c) graphene is covered with a PMMA layer bys pin-coating, d) coating graphene with PMMA and progressive separation from tungsten sheet driven by H 2 bubbles produced at the interface between graphene and Ga-W substrate, e) graphene is transferred to a SiO substrate 2 / Si and f) tungsten sheet is reused as a Ga carrier.

The advantages of this method are its low cost and reproducibility. According to the literature, the specific surface area of graphene synthesized by this method is 2,600 m^2/g, which is higher than that of graphene produced by the mechanical exfoliation method. However, this specific surface area depends on factors such as the size of the metal film used, as well as temperature and pressure, which are key elements for growth [31].

iii. Synthesis of Graphene by Thermal Decomposition of Sic (Epitaxial Growth)

A third graphene synthesis method described in the literature involves heating the surface of a silicon carbide (SiC) substrate in an ultra-high vacuum (UHV) environment to a temperature close to 1,250 °C to sublimate the silicon [34,35]. This process allows for the in situ formation of graphene to be observed using reflection high-energy electron diffraction (RHEED) [36]. This method is reproducible, and the growth of graphene can be controlled by adjusting the time and temperature. Additionally, the graphene synthesized by this method is more homogeneous than that produced by the CVD method, as the surface of the SiC is completely covered by graphene due to multiple reconstructions on the surface [36,37]. Moreover, the SiC substrate is insulating, eliminating the need to transfer the graphene layers to another support.

III. EXFOLIATION OF GRAPHITE SOLUTION

The chemical route is the most suitable technique for large-scale applications in the field of composite materials because it enables the exfoliation of graphite sheets and their subsequent functionalization from the perspective of charge/polymer matrix compatibility [38-46]. The use of intercalating agents and surfactants generally increases the interlayer space in graphite. Surfactants indeed play a crucial role in the exfoliation and stabilization of graphene in polar solvents like water (Figure 6).

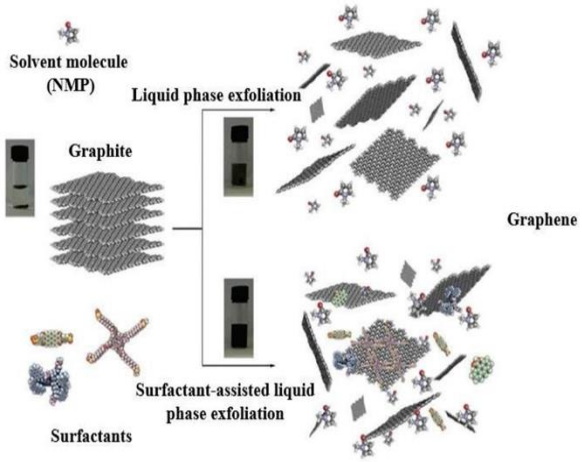

Figure 6: Exfoliation of Graphite in Solution in the Presence (Or not) of Surfactants

For example, Bepete et al. conducted the dispersion of graphite in water to produce graphene monolayers. To achieve a stable and homogeneous dispersion of these monolayers in water, negatively charged graphene solutions were solubilized in tetrahydrofuran (THF) with degassed water, followed by evaporation of the organic solvent. The graphene monolayers obtained were examined using atomic force microscopy (AFM) to confirm their monolayer nature (Figure 7).

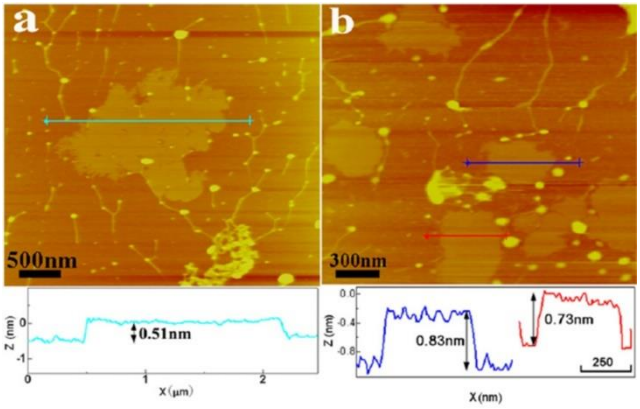

Figure 7: AFM Images of Prepared Graphene Monolayers

Figure 7 depicts topographic AFM images on mica. Figure 7a displays single-layer graphene with a height of 0.34 nm. Figure 7b illustrates the crumpled geometry of large flakes post-deposition. These AFM results confirm the monolayer nature achieved [47].

A. Chemical Functionalisation of Graphite and its Derivatives

i. *Functionalisation of Graphite*

Graphene's excellent electrical conductivity is typically attributed to the absence of a band gap in its electronic structure. Moreover, graphene sheets are insoluble in organic solvents due to reaggregation via π-π interactions between sheets. The most commonly employed solution to address these issues involves using organic or inorganic molecules for the chemical functionalization of graphene [48].

ii. *Non-Covalent Functionalisation*

The principle of non-covalent functionalization of graphite aims to maintain the π-conjugated system. It relies on π-type interactions, electrostatic forces, and/or hydrophobic interactions between the surface of graphene sheets and a "binding partner" molecule. Molecules such as aromatics or surfactants, as well as polymers, can adsorb onto the graphene surface, generating electrostatic repulsion forces that keep the sheets dispersed and prevent reaggregation.

An example of this approach is non-covalent functionalization through the adsorption of pyrene derivatives (Figure 8).

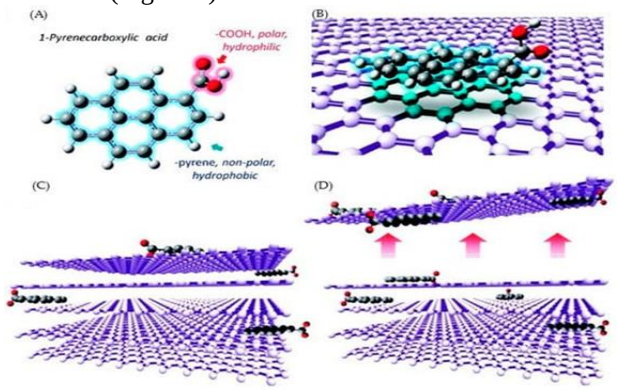

Figure 8: Non-Covalent Functionalization of Grapheneby 1-Pyrenecarboxylic Acid

iii. *Covalent Functionalization*

The chemical modification of the graphene surface involves the rehybridization of sp^2 carbon atoms into sp^3 carbon atoms, disrupting the electronic conjugation and thus the electrical conductivity. Figure 9 summarizes the various options for covalent functionalization reactions of graphene.

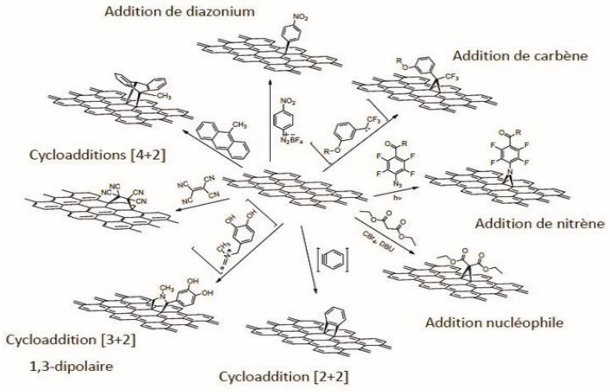

Figure 9: Common Methods of Chemical Modification of Graphene by a Covalent Functionalization

B. Synthesis and Functionalisation of Oxidised Graphite (GO)

i. *Graphite Oxidation*

Oxidized graphite (GO), formerly known as graphitic oxide or graphitic acid, was first prepared by Brodie et al. in 1859. Subsequently, Staudenmaier and later Hummers et al. became interested in the oxidation of graphite using strong mineral acids and oxidizing agents such as KMnO4, KClO3, and NaNO3 in the presence of sulfuric acid (H2SO4) or mixed with nitric acid (HNO3) [49].

This oxidation step of graphite to GO is a key process in the chemical modification of graphite. Graphite oxide consists of stacks of graphene oxide sheets with an interlayer spacing ranging between 6 and 10 Å, depending on the amount of water molecules present between the graphite planes after the oxidation process [50]. The presence of hydroxyl (-OH), carbonyl (C=O), and epoxide (>O) groups on the surface of the sheets, as well as carboxylic acid (-COOH) groups at the edges (as depicted in Figure 10), allows for subsequent chemical functionalization [51-53].

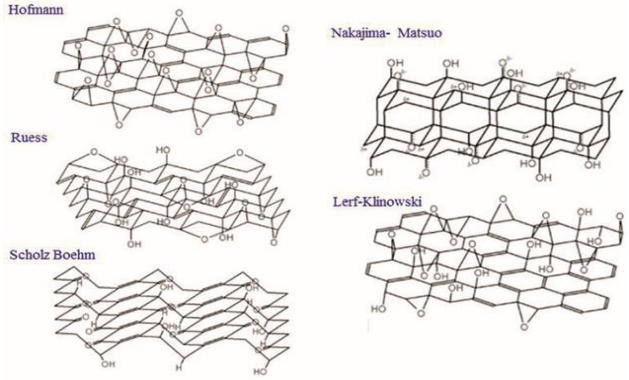

Figure 10: Models Proposed by the Literature for the Structure of the GO

Recently, Gao et al. studied the structure of GO using NMR techniques and showed that the surface of GO contains ketone, lactol (equivalent to a six-membered hemiacetal), tertiary alcohol groups, in addition to epoxide and hydroxyl functionalities.

The production of polymer nanocomposites based on GO derivatives typically involves an exfoliation step of GO prior to its incorporation into polymer matrices.

Exfoliation of GO into individual sheets of oxidized graphene is achieved either in a solvent medium or thermally at high temperatures (>1000°C). The hydrophilic nature and wide interlayer spacing of GO facilitate direct exfoliation in water (or dimethylformamide) through treatment or mechanical agitation, at concentrations up to 3 mg/mL [54]. This technique allows for the preparation of stable colloidal suspensions of oxidized graphene nanosheets [55]. Figure 11 illustrates the synthesis of oxidized graphene from natural graphite.

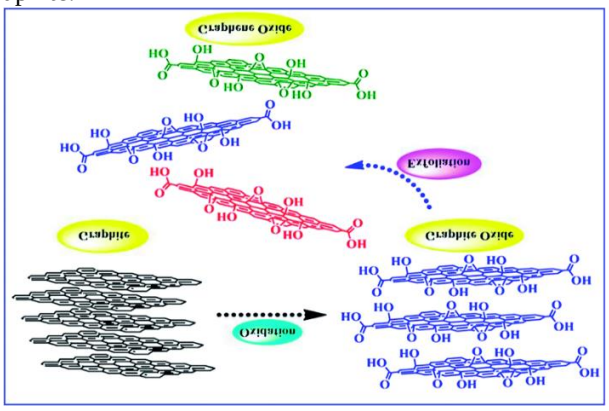

Diagram 1: Synthesis of Oxidized Graphene from Natural Graphite

Zeta potential measurements have indicated that the obtained suspensions are electrostatically stabilized by negative charges, possibly generated by carboxylic groups (-COOH) present on the edges of each sheet of oxidized graphene [56]. However, ultrasonic treatment can fragment the oxidized graphene sheets, leading to a decrease in their lateral dimensions to between 0.1 and 1 µm [57].

Oxidized graphite can also be partially exfoliated into oxidized graphene nanosheets through ultrasonic treatment in organic solvents. Prades et al. demonstrated that GO can exfoliate in tetrahydrofuran (THF), N, N-dimethylformamide (DMF), N-methyl-2-pyrrolidone (NMP), and ethylene glycol (EG) without requiring additional functionalization (Figure 11). Colloidal suspensions of GO obtained at a concentration of 0.5 mg/mL are stable in these solvents and comparable to those in water. They also found that other organic solvents such as methanol, acetone, ethanol, propanol, oxylene, and n-hexane cannot be used to disperse GO effectively (Figure 11).

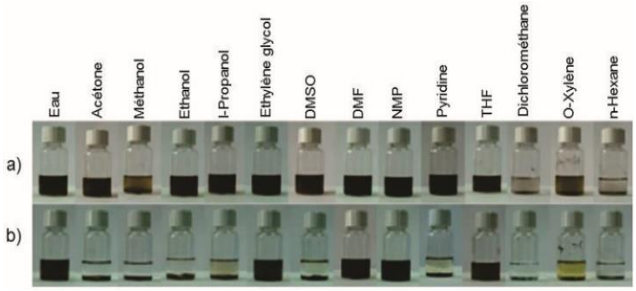

Figure 11: GO Suspensions in different Organic Solvents after Ultrasonic Treatment for 1h: a) Right after Ultrasound Treatment and b) 3 Weeks after Ultrasound Therapy (C=0.5mg/mL)

Additionally, GO can be exfoliated in aprotic solvents through reactions with organic compounds such as octadecylamine or by treatment with organic surfactants [58]. These suspensions are thus suitable for producing polymer/GO nanocomposites.

Mechanical and magnetic agitation are also methods for exfoliating GO into oxidized graphene nanosheets, but they are less efficient compared to sonication.

Due to the chemical structure of oxidized graphene, it is thermally unstable and electrically insulating, which may restrict its use at high temperatures (molten medium) in the production of polymer nanocomposites and in electronic and microelectronic applications. In such cases, partial reduction of oxidized graphene is necessary to restore the conjugated architecture and thereby enhance electrical conductivity and thermal stability. Several methods have been developed in the literature for reducing oxidized graphene, aiming to prepare graphene nanosheets in large quantities with high structural quality and excellent thermal stability.

IV. COVALENT FUNCTIONALISATION OF GO

Chemical functionalization of GO with molecules and/or polymer chains enhances its dispersion in organic solvents. This functionalization involves various classic organic chemistry reactions, and specific examples are provided in Table 1.

Table 1: Different Organic Chemistry Reactions Used for the Functionalization of GO

Type of Chemical Reaction	Change Agent	Responsive Function	Solvent
Nucleophilic addition	3Ğaminopropyltriethoxysilane	Amine on epoxide	DMF
	Dopamine	Amine on epoxide	H2O
	Functionalized ionic liquid amine	Amine on epoxide	Water,DMF,DMS O
	Polyglycerol	Amine on epoxide	Water
Electrophilic addition	Aryl salt ofiazonium of sulphanilic acid	Sulfonation	H2O
	4-Bromo aniline	Bromination	DMF
	Aryl diazonium	Diazotization	DMF
Condensation reaction	Chitosan	Chitosan NH2 with COOH of GO	Water
	SOCl2 followed octadecyl amine	Amine on acyl chloride	THF, DMF
	Alpha, Beta and gamma cyclodextrin	Basic hydroxyl medium with epoxide	Water, DMF, THF
	SOCl2 functionalized amine tracking porphyrin	Amine on the GO-Cl	DMF
Radical addition	Maleic anhydride + peroxide	Radical addition	THF
	Azides	Radical addition	H2O/DMF

Chemical methods of modifying GO can be classified into four categories: nucleophilic additions, electrophilic additions, condensation reactionsand radical additions.

A. Nucleophilic Additions

Chemical modification of GO through nucleophilic addition involves the attack of a pair of electrons (typically from an amine group) on the epoxide group, causing the ring to open and forming a secondary amine and an alcohol group [59]. For instance [60], grafted an alkylamine onto the GO surface via nucleophilic addition of amine groups to the epoxy groups of GO (Diagram 2).

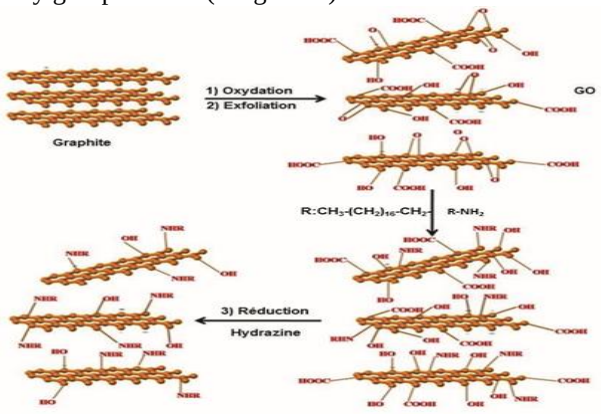

Diagram 2: Functionalization of GO by nucleophilic addition of an alkylamine (Octadecaneamine) on GO followed by a chemical reduction step with hydrazine.

They discovered that the thickness of graphene modified with alkyl amine is approximately 1.5 nm.

Similarly, Yang et al. grafted 3-aminotriethoxysilane onto the surface of GO following Diagram 3.

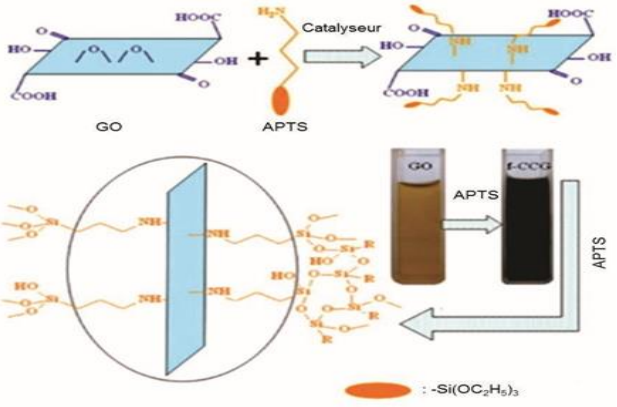

Diagram 3: Functionalization pf GO by 3-Aminotriethoxysilane

Their study demonstrates the effective dispersion of GO modified with 3-aminotriethoxysilane at a concentration of 0.5 mg/mL in various solvents including water, ethanol, dimethylformamide (DMF), and dimethylsulfoxide (DMSO). The ATG analysis reveals a grafting percentage of 10.6% between 550°C and 650°C, or a grafting density near 0.45 mmol/g.

B. Electrophilic Additions

Chemical modification of GO through electrophilic addition often employs diazonium salts (Diagram 4).

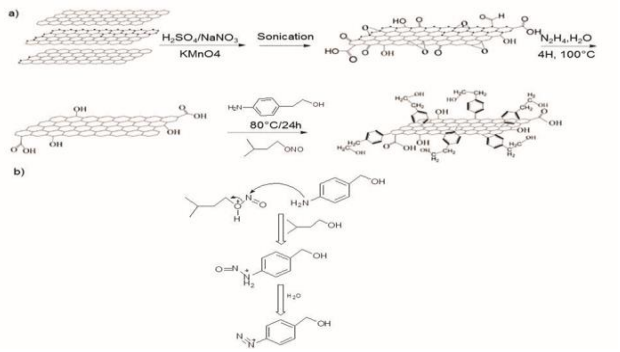

Diagram 4: A) In Situ Formation of a Diazonium Aryl Salt on GO, B) Mechanism of Diazotation

In this study, the grafting percentage of polystyrene onto GO is 82%, corresponding to a grafting density of 0.58 mmol/g. Additionally, the glass transition temperature after this functionalization increased by 15°C compared to pure polystyrene (91.4°C for pure PS, 106.7°C for GO-PS). Furthermore, atomic force microscope (AFM) observation revealed an increase in thickness from 0.73 nm for GO to 3 nm for GO-PS.

C. Condensation Reactions

Condensation reactions involve reactions between two distinct functional groups that result in the formation of a new functional group, often accompanied by the release of a simple molecule such as H_2O or HCl. The chemical modification of GO can selectively target hydroxyl and carboxylic acid groups. For instance, A. Ashori et al. grafted ethylenediamine (EDA), 4,4'-diaminodiphenyl sulfone (DDS), and p-phenylenediamine (PPD) onto GO (Figure 12).

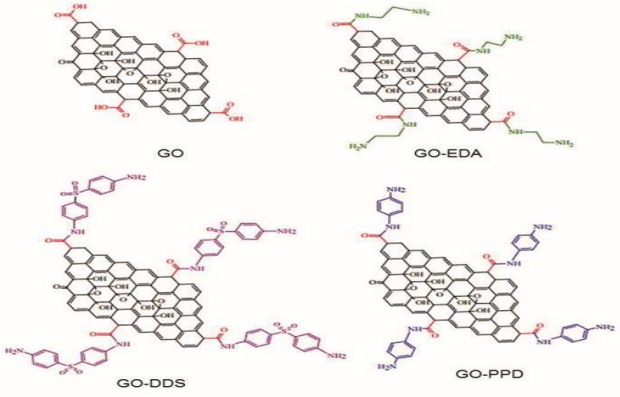

Figure 12: Chemical Modification of GO By EDA, DDS and PPD

Various characterization methods were employed to assess these functionalizations, confirming the oxidation of GO and its subsequent chemical modification. The reduction in oxygenated functional groups and the presence of amino groups were evaluated using FT-IR spectroscopy and elemental analysis. Additionally, the impact of adding GO and functionalized GO on the mechanical properties of the composite was evaluated, demonstrating that GO functionalized with ethylenediamine (GO-EDA) at a concentration of 0.3% by weight can enhance tensile strength.

D. Radical Additions

The carbon-carbon double bonds in the chemical structure of GO can also undergo radical additions. For instance, Guimont et al. conducted radical grafting of pentadecane by abstracting hydrogen atoms from GO (Diagram 6).

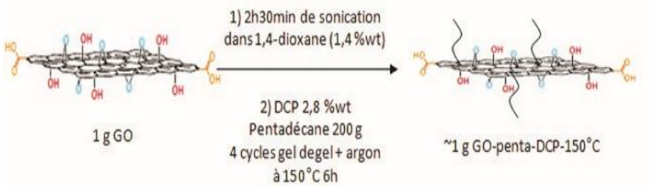

Diagram 6: Grafting of Pentadecane onto GO in the Presence of a Peroxide

Their ATG analysis confirmed the phenomenon of solvothermal reduction, showing a decrease in mass loss around 200°C, which is associated with the pyrolysis of polar functional groups after grafting and/or heat treatment at 150°C. This ATG analysis was used to assess the grafting efficiency of pentadecane on GO. The mass loss between 300°C and 500°C for GO- pentadecane with dicumyl peroxide (DCP) at 150°C (GO-penta-DCP-150°C) was compared to GO treated at 150°C in pure pentadecane. The difference in mass loss between 300°C and 500°C was only 1%, falling within the uncertainty of the ATG measurement, making it difficult to accurately evaluate the grafting efficiency. Furthermore, the morphology of GO-penta-DCP-150°C was observed via SEM to highlight its sheet-like structure. Additionally, Hsiao et al. conducted radical addition of maleic anhydride grafted onto poly(oxyalkylene) amine with a molecular weight of 2000 (MA-POA2000) in the presence of benzoyl peroxide (BPO) on GO previously thermally reduced (Diagram 7).

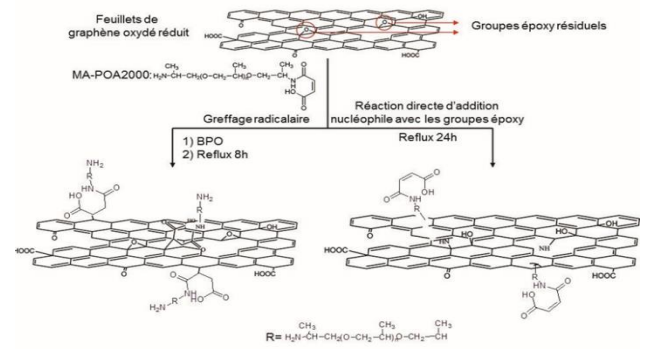

Diagram 7: Radical grafting of a maleic anhydride grafted on poly(oxyalkylene)amine with a molecular weight of 2000 (MA-POA2000) on a thermally reduced GO in the presence of benzoyl peroxide (BPO).

In this study, they confirmed that MA-POA2000 functionalized graphene exhibits homogeneous dispersion in THF at a concentration of 0.25 mg/mL for over two months, unlike thermally reduced graphene which retains residual epoxy groups. This indicates that the long MA-POA2000 chain effectively enhances compatibility between graphene and THF. Additionally, ATG analysis revealed a grafting efficiency of 17.8% for radical grafting and 17.2% for direct nucleophilic addition, corresponding to grafting densities of 0.089 mmol/g and 0.082 mmol/g, respectively.

The grafting of polymer chains onto oxidized graphene is widely employed through onto, from, and through grafting techniques.

E. Grafting Onto Grafting Polymers

The principle of the "Grafting onto" technique involves coupling functional polymer chains to a substrate using complementary functional groups (Figure 13).

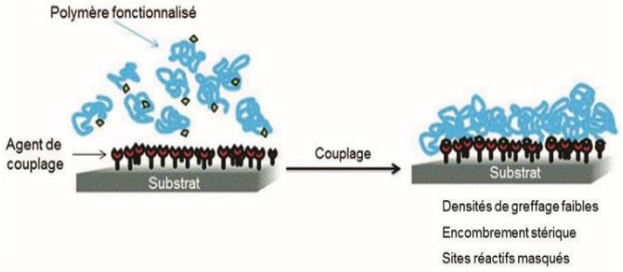

Figure 13: Principle of the "Grafting Ongo" Technique

Generally, this grafting method results in low grafting densities because the initially grafted chains spread across the surface, covering the reactive sites of the substrate.

F. Grafting Through Polymers

The "Grafting through" technique involves initially grafting a "monomer" (such as a double bond) onto the substrate surface, followed by polymerization of the monomer both on the substrate surface and in the solution (Figure 14).

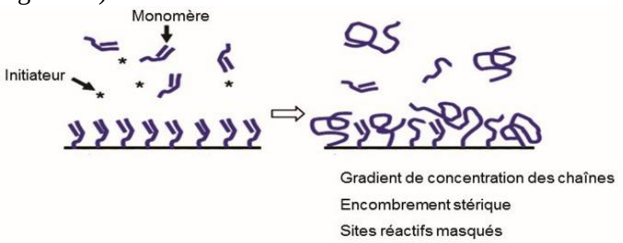

Figure 14: Mainprinciple of the "Grafting Through" Technique

G. Grafting from Grafting Polymers

in the "Grafting from" technique, anionic or radical active sites are first generated on the substrate surface, which are then utilized to initiate the polymerization of a monomer (Figure 15).

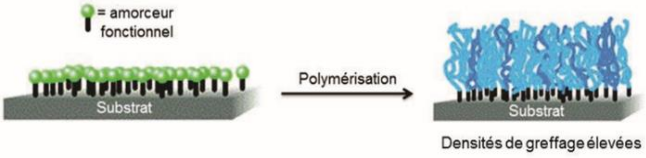

Figure 15: Principle of the "Grafting From" Technique

This method leads to higher grafting densities than the grafting onto technique.

H. Reduction of Oxidized Graphite Derivatives

i.Thermal reduction after functionalization

The synthesis of graphene nanosheets through GO reduction was initially reported by Schniepp et al. However, thermally reduced graphene nanosheets can also be obtained by rapidly heating GO in an inert, high-temperature environment. Heating GO to 1050°C for 30 seconds in such conditions results in both exfoliation and reduction of GO (Diagram 8).

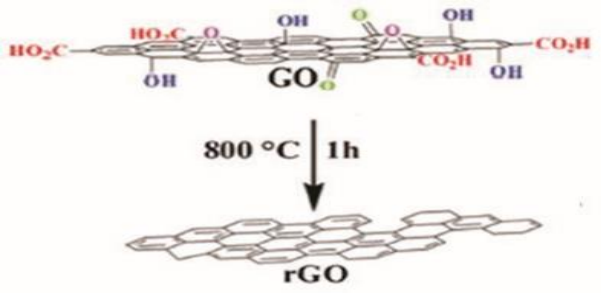

Diagram 8: Production of Graphene from the Thermal Reduction of GO

Exfoliation of GO occurs due to the pressure generated by CO2 gas released from the decomposition of carboxylic acid (COOH) and epoxide (I>O) groups present on GO. The advantage of this method is that exfoliation and reduction are achieved in a single step, allowing graphene to be obtained without the need for a prior dispersion step of GO in organic solvents.

ii.Chemical reduction

The chemical reduction of GO begins with a stable colloidal dispersion of functionalized GO or GO itself.

Methods described in the literature typically involve the use of hydrazine or its derivatives like dimethylhydrazine. Chemical reduction using hydrazine or its derivatives reduces the oxygen groups on the surface and edges of GO, typically resulting in graphene nanosheets without structural defects. Stankovich et al. proposed a mechanism for reducing epoxide functions with hydrazine (Figure 16).

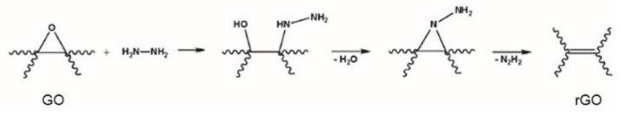

Figure 16: Proposed Mechanism for Chemical Reduction of GO to Rgo by Hydrazine

Hydrazine and its derivatives (such as dimethylhydrazine and hydrazine hydrate) are renowned for their effectiveness as reducing agents. However, due to its toxicity and high cost, hydrazine is not widely utilized in industrial settings. Consequently, alternative experimental protocols are proposed in the literature to circumvent its use. Chemical reduction of colloidal suspensions of GO can also be achieved using various other chemical reducing agents, such as hydroquinone, sodium borohydride, sulfur compounds, UV-irradiated TiO2, Vitamin C, iron, sodium hydroxide, amino acids, alcohols, sugars, hydroiodic acid, and other metal powders.

I. Main Methods for Characterising Graphene Derivatives

After graphite oxidation, and possibly its functionalization, various characterization techniques are employed, including spectroscopy (UV-Vis, IR, Raman, XPS, XRD, thermogravimetric analysis (TGA)) and microscopy (SEM, TEM, AFM).

i. Spectroscopic analyses

Infrared (IR) spectroscopy is employed for determining the chemical composition of bonds within materials (Figure 17.A).

X-ray diffraction (XRD) confirms the insertion of chemical groups between graphite and/or graphene oxide (GO) sheets, as well as verifies the exfoliation of graphene nanosheets (Figure 17.B).

Raman spectroscopy assesses changes in hybridization, such as the transition from sp^3 to sp^2 during the reduction of GO, and quantifies the number of sheets involved in aggregations (Figure 17.C).

X-ray photoelectron spectroscopy (XPS) quantifies the elemental composition (e.g., oxygen, nitrogen, carbon) on the surface of graphite derivatives and identifies the types of bonds present in the structure of GO. Additionally, XPS is utilized to investigate chemical modifications and reductions of GO (Figure 17.D).

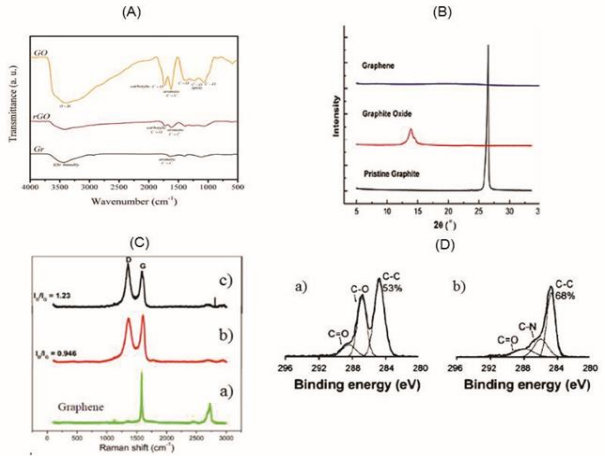

Figure 17: (A) Infrared Spectroscopy of Graphite, GO and rGO. (B)

X-ray diffraction of graphite, GO and graphene. (C) Spectroscopy of

RAMAN for a) graphene, b) GO, and c) rGO. (D) Photo spectroscopy

electronic-X (XPS) C1s for a) GO and b) rGO .

UV-vis spectroscopy is utilized to confirm the chemical reduction of graphene oxide (GO) and can also assess the dispersion of graphene-based nanocomposites in solvents (Figure 18.A).

Thermogravimetric analysis (TGA) offers insights into the quantity of grafted organic matter, the thermal stability of graphene-based nanocomposites, the reduction process of GO, and the rate of pyrolysis of oxygen-containing groups within the final structure of GO (Figure 18.B).

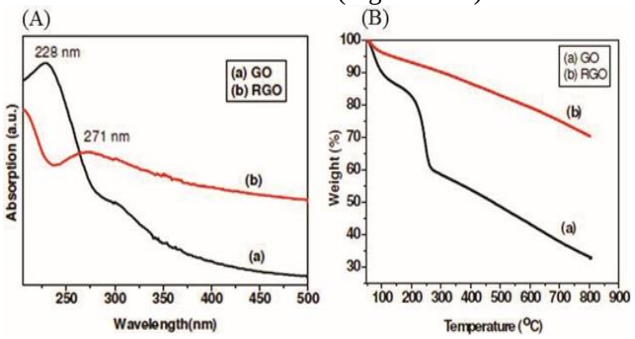

Figure 18: (A) UV-Visible Absorption Spectra for a) GO and b) rGO. (B) Analysis thermogravimetric (ATG) for a) GO and b) rGO

ii. Microscopy

The atomic force microscope (AFM) is employed to evaluate the lateral dimensions, thickness, topography, and structural defects of the substrate under study.

The scanning electron microscope (SEM) offers a qualitative assessment of the three-dimensional structure and morphology of graphene sheets.

The transmission electron microscope (TEM) is utilized to determine the size of graphene nanosheets and can distinguish between individual sheets and multi-sheet aggregations.

iii. Polysaccharides

Polysaccharides are natural polymers composed of multiple sugar units linked by glycosidic bonds. They exhibit covalent sequences ranging from 20 to several thousand monosaccharide units. The diversity of polysaccharides found in nature reflects their varied properties and potential applications. Plant-derived polysaccharides include starch, cellulose, pectins, and gums. Algal sources provide polysaccharides such as alginates, carrageenans, agar, and fucans. Polysaccharides of animal origin include heparin and chondroitin, while microbial sources yield polysaccharides like dextrans and xanthans.

iv. Cellulose

Cellulose is the most abundant polymer on Earth, constituting approximately 50% of biomass with annual global production by plants ranging from 50 to 100 billion tons. It serves as the primary component of plant cell walls and wood, comprising up to 95% in cotton fibers and 40 to 55% in wood. Cellulose is a linear polymer composed of glucose units linked together by β-1,4-glycosidic bonds, with cellobiose as its repeating unit motif (Figure 20).

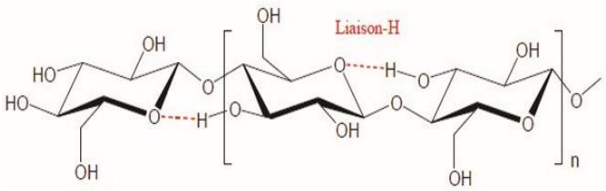

Figure 19: Chemical Structure of Cellulose

Cellulose exhibits a highly resilient three-dimensional structure due to the presence of intra- and intermolecular hydrogen bonds facilitated by its glycosidic bonds. However, cellulose possesses a crystalline and rigid structure that is relatively inert and insoluble in many organic solvents. Moreover, cellulose is composed of crystalline regions organized into microfibrils alongside amorphous regions, which exhibit greater reactivity. Cellobiose, consisting of two β-D-glucopyranose units (anhydroglucose units or AGUs) in a chair conformation linked by β (1→4) glycosidic bonds, contributes to its linear structure (Figure 20).

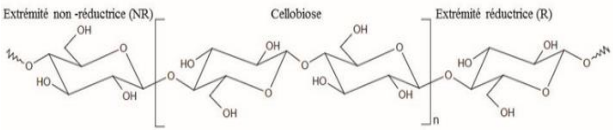

Figure 20: Representation of a Cellulose Chain

The reducing end (R) of the cellulose polymer refers to the anhydroglucose unit (AGU) where the anomeric carbon is not involved in a glycosidic bond with another carbohydrate unit (Figure 20).

Conversely, the glucose unit at the opposite end of the cellulose chain is termed the non-reducing end (NR) because its anomeric carbon is linked via a β (1→4) glycosidic bond (Figure 20). The number of AGU units defines the degree of polymerization (DP) of cellulose, which ranges from 400 to 14,000. The highest DP is observed in native cellulose, which has not undergone chemical treatment. Typically, purified celluloses have an average DP of 2,500.

v. Physico-Chemical Characteristics of Cellulose

Cellulose exhibits both crystalline and amorphous regions, with a higher density of hydrogen bonds found within the crystalline zones. The crystallinity of cellulose varies: it ranges from 40 to 50% in wood, approximately 60% in cotton, and exceeds 70% in certain types of seaweed.

vi. Cellulosic Chain Cohesion

AGUs have three hydroxyl groups including two secondary alcohol functions (in position 2 and 3) and a primary alcohol function (in position 6) (Figue.21A).

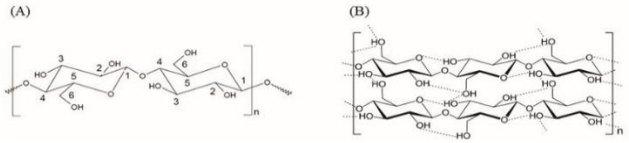

Figure 21: (A) Numbering of the Carbons of an AGU unit, (B) Intra Hydrogen Bonds and Cellulose Intermolecular

These hydroxyl groups, along with the glycosidic bonds, are positioned in the equatorial orientation relative to the plane of the glucopyranose ring (Figure 21A). This conformation facilitates the formation of both intra- and intermolecular hydrogen bonds (Figure 21B). The presence of these hydrogen bonds results in several consequences. Firstly, due to their numerous and organized arrangement, they impart a very high mechanical strength to cellulose fibers. Additionally, cellulose is highly insoluble because disrupting these interactions is challenging. Finally, cellulose is non-fusible because the temperature required to break these hydrogen bonds exceeds that required for the chain's decomposition, which occurs through the rupture of the glucopyranose ring.

vii. Bulking Properties

Cellulose exhibits two distinct characteristics, crystalline and amorphous, which influence solvent penetration through two stages. The initial and easier stage involves penetration into the amorphous regions, inducing intercrystalline swelling. If the solvent manages to diffuse into the crystalline regions, it causes intracrystalline swelling. However, not all solvents can penetrate the crystalline zones; for instance, water induces only intercrystalline swelling of cellulose fibers.

The maximum water uptake capacity in the cell walls of wood cells (saturation point) varies between 0.31 and 0.62 grams per gram of dry matter.

This capacity varies depending on cellulose origin, processing methods, and the history of drying and rewetting. Intercrystalline swelling has also been observed with organic solvents. Protic and aprotic solvents, in combination with water, exhibit greater swelling capabilities compared to alcohols (such as formamide, dimethyl sulfoxide, and ethanolamine).

Certain compounds can penetrate the crystalline barrier and induce intracrystalline swelling without dissolving cellulose. Examples include alkaline salt hydroxides (such as soda ash used in mercerization), amines, and liquid ammonia. These products, which induce both inter- and intracrystalline swelling of cellulose, find application in heterogeneous phase reactions.

viii. Cellulose solubilisation methods

Cellulose is a polysaccharide known for its high resistance to dissolution. However, certain solvents have the capability to dissolve cellulose chains by disrupting hydrogen bonds. Cellulose solvents are classified based on their chemical nature or their capacity to modify cellulose, often referred to as "derivatizing" solvents.

ix. Solubility in water

Cellulose is insoluble in water and most common organic solvents, with only a limited number of specific solvents capable of dissolving it. The solubility of cellulose correlates directly with its degree of polymerization (DP), as higher DP values result in increased intermolecular hydrogen bonding. The solubility classification of cellulose in water is divided into three zones (Figure 22):

- Cellulose with DP > 30 exhibits polymer-like behavior.
- Cellodextrins with 7 < DP ≤ 13 can be dissolved in water under specific conditions.
- Cellodextrins with DP < 7 are water-soluble.

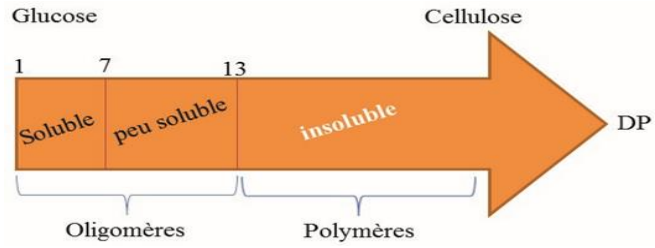

Figure 22: Solubility of Cellulose in Water According to its DP

x. Solubilisation of cellulose by molecular interactions

There are solvents capable of dissolving cellulose through intermolecular interactions, classified into two categories: aqueous and non-aqueous media. Aqueous solvents include inorganic salts like lithium chloride derivatives or molten salts, as well as complexes with transition metals such as cuppramonium hydroxide (Cuam) or cupriethylenediamine hydroxide (Cuen), and ammonium hydroxides or alkaline lins. Industrial processes like dissolution in Cuam utilize these aqueous solvents for large-scale applications. Non-aqueous, non-derivative solvents include N-oxides such as N-methylmorpholine-N-oxide (NMMO) and N,N-dimethylacetamide (DMAC) in the presence of lithium chloride (DMAC/LiCl) (Figure 23).

Figure 23: Chemical Structures of Cellulose Solubilization Solvents

xi. Solubilisation of cellulose by chemical modification

Cellulose-derived solvents are methods that alter the chemical structure of cellulose through the formation of ester, ether, or acetal intermediates to facilitate dissolution. Additionally, these modified products can be precipitated and utilized for their functional properties. Commonly used derivatives include cellulose acetate (used in films, membranes, and filters), cellulose nitrate (employed in explosives), and cellulose xanthate (used in viscose and cellophane production).

xii. Mechanical Properties of Cellulose

Recent studies by numerous researchers have investigated the mechanical properties of cellulose, particularly its role as a reinforcing material in composites. The mechanical properties and thermal stability of cellulose are governed by inter- and intramolecular hydrogen bonds (Fig. 24). The macromolecular chains are connected via intermolecular hydrogen bonds along the a-axis, forming sheets. These sheets are further held together by Van der Waals forces along the b-axis (Fig. 25).

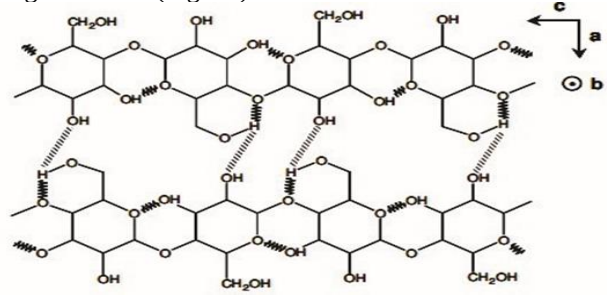

Figure 24: Inter- and Intra-Molecular Hydrogen Bonds in Cellulose

Cellulose exhibits strong anisotropy within the plane defined by axes a and b, which is perpendicular to the c-axis, the axis of its chains (Figure 25). Recently, researchers have endeavored to determine the elastic constants of crystalline cellulose through experimental methods or simulations. This approach involves measuring deformations in the cellulose crystal lattice using X-ray diffraction (XRD) under stress applied along specific axes in oriented samples. Molecular modeling has also enabled theoretical calculations of these constants, considering the presence of inter- and intramolecular hydrogen bonds. Kroon-Batenbur et al. and Tashiro and Kobayashi calculated modulus values of 136 and 167 GPa, respectively, for native cellulose, accounting for hydrogen bonds. Without considering hydrogen bonds, these values were reduced to 89 and 70 GPa, respectively. These theoretical calculations align closely with experimental values, affirming the significant role of hydrogen bonds.

Tashiro also evaluated the mechanical property anisotropy perpendicular to the chain axis, estimating Young's modulus at 54 GPa along the a-axis (where intermolecular hydrogen bonds are prominent) and 15 GPa along the b-axis (where Van der Waals interactions dominate).

xiii. Grafting of Cellulose onto Substrates

3/4 **Grafting of Cellulose onto Titanium Dioxide**

Anirudhan et al. developed a TiO2 surface grafted with glycidyl methacrylate functionalized aminocellulose (Et-AMPGDC) to prepare an adsorbent material capable of removing arsenic (V) [As (V)] from aqueous solutions. The pH of the solution is a critical factor influencing the adsorption behavior of this system. Anirudhan investigated the impact of pH variation (ranging from 2.0 to 9.0) on the adsorption efficiency of As(V) onto Et-AMPGDC, using initial concentrations of 25 and 50 mg/L (Figure 25).

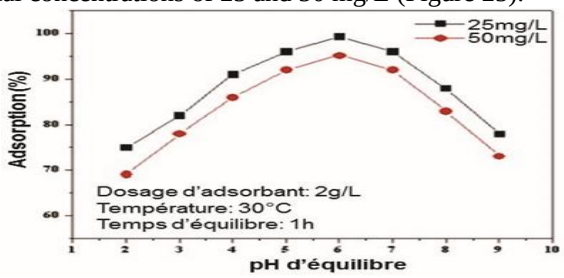

Figure 25: Effect of Ph Variation on the Percentage of Adsorption of as(V) on Etampgdc

pH measurements of the solution at different initial concentrations show that the optimal adsorption is noted at pH = 6. Thus, the adsorption of As (V) on Et-AMPGDC at an initial concentration of 25 and 50 mg / L is respectively99.3% and 95.2% at pH 6.0.

xiv. Areas of Application of Cellulose

3/4 **Application as Reinforcement for Paper**

Cellulose has recently garnered significant interest as an additive to enhance the physical and mechanical properties of paper, showing promising potential in paper and packaging technology applications. In a separate study, Gonzalez et al. demonstrated that combining enzymatic pulp treatment (biobeating) with cellulose addition offers a promising alternative to improve the mechanical properties of paper without compromising drainage rates to undesirable levels.

The incorporation of cellulose into enzyme-treated pulp enhances the mechanical properties of paper, albeit with a reduction in porosity while maintaining opacity unchanged. Cellulose effectively promotes the adhesion of cellulose fibers, a hypothesis substantiated by field emission scanning electron microscopy (FE-SEM) analysis (Figure 26A). MFC: Micro cellulose fiber.

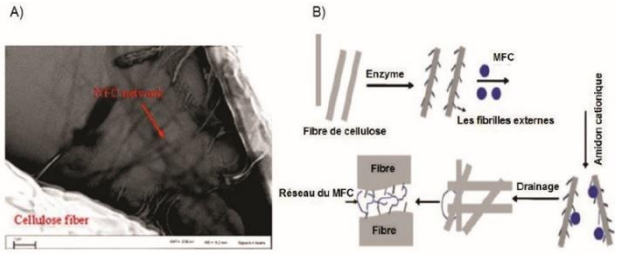

Figure 26: A) SEM-EC Image of a Layer of Phosphate Prepared in the Presence of Cellulose Nanofibers B) Mechanism of Paper Reinforcement by Cellulose

Thus, the cellulose reinforcement mechanism for paper has also been proposed (Figure 27B).

3/4 **Applications for the Development of Conductive Materials**

Due to its high functionality, specific surface area, excellent mechanical properties, and non-toxic nature, cellulose presents numerous industrial applications in the realm of conductive materials.

For instance, Mihranyan et al. synthesized a conductor composite based on polypyrrole and cellulose derived from Cladophora sp., a green algae. This composite was prepared by polymerizing pyrrole in the presence of iron (III) chloride (FeCl3) on a polysaccharide substrate extracted from algae. The specific surface area of the composite material was determined to be 57 m2/g, and the fibrous structure of cellulose remained intact even after depositing a 50 nm thick layer of polypyrrole. Moreover, the composite exhibited excellent stability over cycles when used as an electrode. This material shows promise for various electrochemical applications, including ion exchange, separation devices, and sensors. Additionally, there is increasing interest in lithium (Li) batteries as an energy storage system. However, to facilitate their widespread adoption, barriers beyond performance and safety enhancements must be addressed. Efforts are underway to develop environmentally conscious production systems that integrate the use of sustainable materials, enabling the cost-effective production of large-area devices that are easily recyclable.

xv. Chitosan

Chitosan, derived from chitin, is a polysaccharide that ranks among the most abundant natural polymers on Earth, alongside cellulose. Chitin is predominantly found in the animal kingdom among invertebrates (such as insects, crustaceans, and cephalopods), in certain algae cell walls within the plant kingdom, and in various fungi (including yeast, penicillium, and mushrooms). Discovered by Henri Braconnot in 1811, it consists of N-acetyl-D-glucosamine (GlcNAc) saccharide units linked by β (1→4) bonds. The primary industrial sources of chitin and chitosan today are crustacean shells (e.g., shrimp) and the endoskeletons of squid. The chemical structure of chitin is depicted in Figure 27.

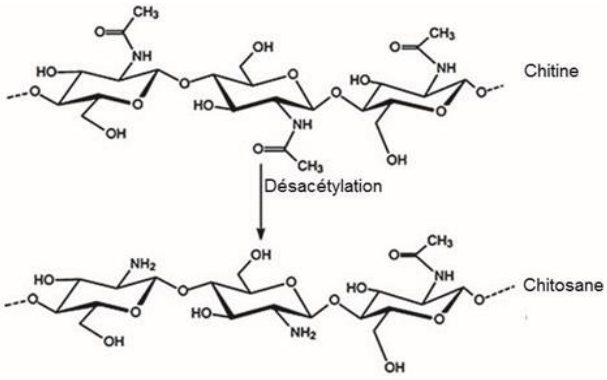

Figure 27: Chemical Structure of Chitin and Deacetylated Chitin (Chitosan)

Commercially available chitin is not solely composed of GlcNAc due to partial deacetylation through chemical extraction processes. Typically, these products consist of copolymers containing both GlcNAc and glucosamine (GlcN) units. Therefore, understanding the concept of degree of acetylation (DA) becomes crucial, representing the molar fraction of GlcNAc units within the polymer structure.

Some researchers prefer using the degree of deacetylation (DD), which is directly related to DA through the relationship DD = 1 - DA. Chitosan is produced by deacetylating chitin through a reaction involving concentrated sodium hydroxide at elevated temperatures (T = 90°C). This process may be repeated up to four times to achieve complete deacetylation, resulting in a chitosan with DA = 0.

However, this deacetylation treatment typically leads to a significant reduction in molecular weight, decreasing from approximately 500,000 g/mol to 75,000 g/mol. Achieving a low DA often comes at the expense of molecular weight.

The distinction between chitin and chitosan is commonly defined by DA:

- For DA > 60%, the material is referred to as chitin.
- For DA < 60%, it is categorized as chitosan.

This classification is somewhat arbitrary and may vary among researchers. Chitin and chitosan, both derived from biomass, exhibit varying physicochemical properties such as average molecular weight and distribution of GlcNAc units, impacting their solubility depending on their sources.

xvi. *Properties of Chitosan*

Solubility

Chitosan exhibits insolubility in organic solvents and in neutral to basic pH water due to extensive hydrogen bonding among its hydroxyl, amine, acetamide, and ether groups [60]. Conversely, it becomes soluble in acidic conditions, typically in a 1% acetic acid solution, due to protonation of its free amine groups. This protonation increases electrostatic repulsion among the positively charged amines, which outweighs attractive intra- and inter-chain interactions such as hydrogen bonding and hydrophobic effects, thereby enabling chain solvation. The solubility of chitosan is primarily governed by the hydration of these protonated sites and the acid-base properties of its amine groups, described by the following equilibrium:

$$R\,NH\,2 + H_3W + R\,NH_3^{+} \rightleftharpoons + H_2O$$

(R: chitosan chain)

xvii. *Grafting of Chitosan onto Substrates*

3/4 **Grafting of chitosan onto a titanium dioxide surface**

Chitosan is a highly suitable material for use as a bioactive coating on medical implant materials. In this study, a photoelectron spectroscopy (XPS) analysis was conducted on coatings prepared from chitosan that was 86.4% deacetylated and applied onto implant-grade titanium. The process involved a three-step procedure for attaching chitosan films: first, deposition of 3-aminopropyltriethoxysilane (APTES) in toluene; second, reaction between the amine end of APTES and glutaraldehyde; and finally, reaction between the aldehyde end of glutaraldehyde and chitosan (Figure 28).

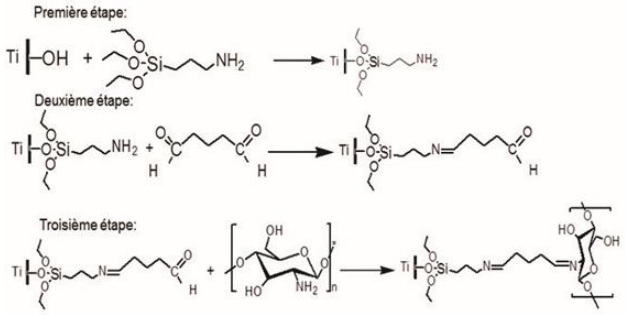

Figure 28: Different Steps of Grafting Chitosan on a Titanium Surface

Each step of synthesishas been studied by XPS to verify the structure and chemical forms of the detected elements.

xviii. *Mechanical properties and applications*

Chitosan is derived from chitin through deacetylation, removing sufficient acetyl groups (CH3-CO) to render the polymer chain soluble in most dilute acids. This modification imparts chitosan with a cationic nature, particularly advantageous in acidic environments. Despite being solid and translucent, chitosan is insoluble in water, alcohols, and ethers, owing to hydrogen bonding within its structure, which contributes to its excellent mechanical and thermal properties. Key parameters defining chitosan include viscosity and degree of deacetylation (DA), representing the molar fraction of acetylated N units, influencing its physicochemical properties such as molecular weight, solubility, mechanical strength, and thermal stability. Controlled manipulation of these parameters facilitates the production of a diverse range of chitosan and derivative products applicable in medical and industrial applications.

In the medical field, chitosan serves as a hemocompatible material, finding use in artificial skin for wound healing acceleration, bioresorbable sutures due to its strength and flexibility, and as components in contact lenses. Additionally, chitosan is extensively utilized in composite materials as a polymer matrix for dispersing graphene nanoparticles. Its film-forming properties and non-toxic nature also make chitosan and its derivatives valuable in cosmetics and food industries. Moreover, chitosan is employed in paper manufacturing to produce moisture-resistant papers and plays a pivotal role in treating water contaminated with heavy metals and polychlorobiphenyls, acting as an excellent chelating agent. Its biodegradable nature further enables its application in drug encapsulation and delivery systems.

xix. *Biodegradability*

The biodegradability of a material significantly influences its long-term performance in various applications. Chitosan undergoes degradation in biological environments primarily through enzymatic and non-enzymatic hydrolysis processes. Enzymes such as lysozymes are primarily responsible for enzymatic degradation of chitosan, targeting the more acetylated regions of the polymer chain. This enzymatic action results in the formation of chitosan oligomers as degradation products.

The rate of chitosan degradation is dependent on its degree of deacetylation (DA), which also impacts the crystallinity of solid physical forms and hydrogels. Low DA chitosan exhibits slower degradation kinetics, whereas high DA chitosan degrades more rapidly. Additionally, factors such as the presence of nitric oxide (NO), which plays a significant role in immunosuppression following severe burns, can influence the degradation pathways of chitosan in biological contexts.

xx. Polysaccharide bio composites

A composite material is formed by combining two or more immiscible materials with a strong bonding capacity. The concept behind composite materials is to integrate materials with complementary properties to synergistically enhance their overall performance, encompassing mechanical, thermal, electrical, and chemical attributes. In composite materials, two primary components are always present: the reinforcement and the matrix. The quality of a composite material largely hinges on the nature of its constituents and the interface quality between the reinforcement and the matrix, which critically influences mechanical properties. Therefore, meticulous control over fabrication processes is as crucial as selecting appropriate constituents.

Matrix materials in composite structures, particularly organic matrices or polymeric matrices, offer commendable mechanical strength, corrosion resistance, and sometimes favorable electrical and dielectric properties. However, they typically exhibit limited resistance to high temperatures and fire hazards. Conversely, metal matrix composites boast excellent thermal resistance alongside good electrical and thermal conductivity. Ceramic matrix composites (e.g., C, Al2O3, SiO2, Cr2O3, MgO, SiC) are developed to mitigate the inherent brittleness of ceramics, thereby enhancing material toughness.

The role of reinforcement within composites is pivotal for ensuring mechanical functionality. Reinforcements can take the form of particles or fibers and may be categorized into inorganic types such as glass, silica, carbon, and ceramics, or organic types like polyester, polyamide, and natural fibers derived from plants or animals. Various reinforcement architectures can be employed based on desired mechanical properties, including one-dimensional orientations where fibers align in a single direction, two-dimensional structures such as woven or non-woven fabrics, three-dimensional configurations involving preformed volumes with fibers oriented in multiple spatial directions, and random multidirectional arrangements where fibers are disordered or agglomerated with a binder.

Biocomposites utilize reinforcements derived from animal or plant sources, often incorporating polysaccharides due to their specific advantages like low density and favorable mechanical properties. These biocomposites find applications across diverse fields, as illustrated in Figure 29.

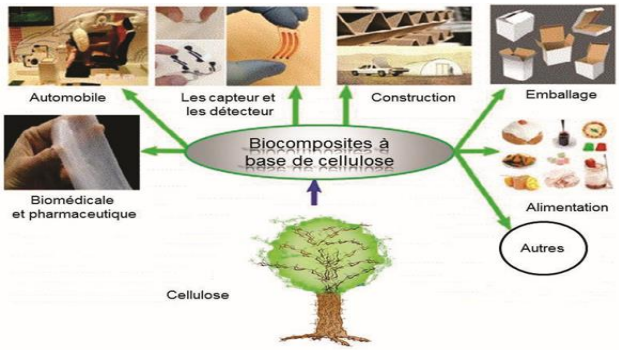

Figure 29: Different Applications of Bio Composites

Physico-Chemical Properties

Recent research has focused on the development of cellulose-based biocomposites and/or chitosan for various applications. Davoodbasha et al. synthesized chitosan-based nanobiocomposites incorporating silver nanoparticles (AgNPs) at varying concentrations for biomedical applications. Corsello et al. investigated the morphology and properties of biocomposite films based on chitosan and nanocrystalline cellulose dispersed in a NaOH solution. Additionally, Chen et al. prepared biocomposites with unique properties using ionic assembly between anionic carboxymethylcellulose and cationic copolymers like PDMAPMA and PLA. Figure 30 depicts the synthesis processes of these biocomposites.

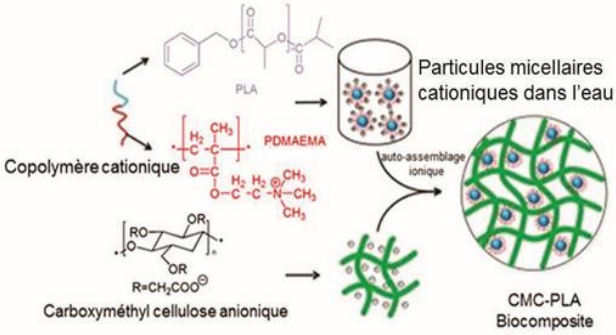

Figure 30: Synthesis of Bio Composites by Ionic Assembly Between Cellulose Microcrystalline (CMC) and PLA-b-PDMAEMA

The results of scanning electron microscopy (SEM) andinfrared spectroscopy (FTIR) showed the interaction between quaternized copolymer micelles and anionic CMC lattices (Figure 31 A and B).

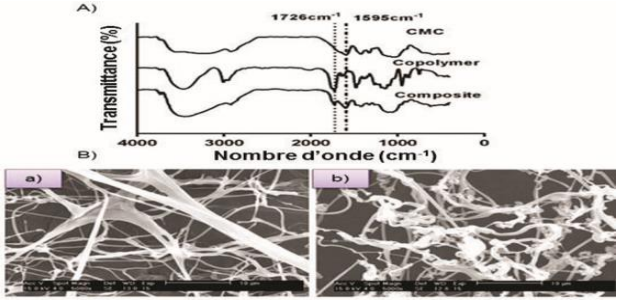

Figure 31: A) Infrared Spectrum, B) Scanning Electron Microscope Images a) of the CMC Cellulose and (b) Bio Composite

Infrared spectroscopy was employed to investigate interactions within the cationic copolymer, anionic carboxymethylcellulose (CMC), cellulose lattice, and the CMC/PLA biocomposite. The absorption bands observed around 3500 cm^-1 and 3000 cm^-1 in all three samples correspond to O-H groups of residual water molecules and C-H groups (Figure 31A). Additionally, prominent peaks observed at 1595 cm^-1 and 1726 cm^-1 indicate the presence of C-O bonds and carboxyl and ester groups, respectively. Specifically, in carboxymethylcellulose, all C-O bonds exist as carbonyl, evidenced by the peak at 1595 cm^-1. Conversely, the copolymer exhibits a strong peak at 1726 cm^-1, attributed to C-O bonds in the ester groups of the copolymer. Furthermore, scanning electron microscopy (SEM) reveals individual fibrils forming a network in the CMC cellulose suspension, while addition of the cationic copolymer PLA-b-PDMAEMA causes fibrils to aggregate. Moreover, spherical particles on the surface of cellulose nanofibers coalesce, forming bridges that confirm interactions between anionic CMC cellulose and cationic copolymers in the biocomposite formation.

xxi. Grafting of Polysaccharides on a Graphitic Substrate

In this part, we will discuss the most effective techniques that are commonly used for the manufacture of nanocomposites based on polysaccharides and graphene.

xxii. Direct Grafting of Cellulose onto Oxidized Graphite Non-Covalent Approach

Many researchers have been interested in grafting cellulose onto the surface of GO to improve physical, chemical and thermal properties by different grafting methods . For example, adsorbed cellulose to the surface of oxidized graphite via hydrogen bonds between the oxygen atom of the carboxylic acid function of GO and the hydrogen atom of the hydroxyl function of cellulose (Figure 32A).

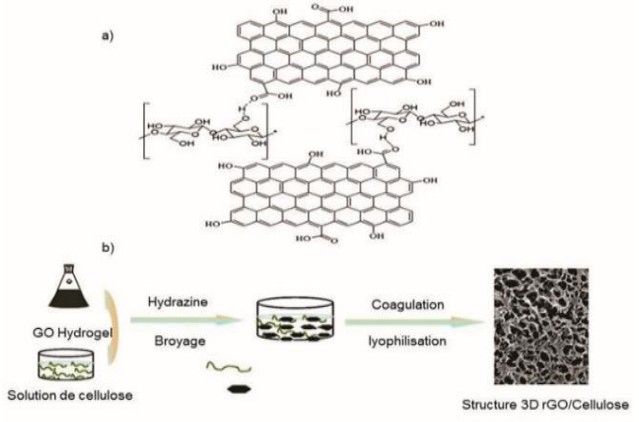

Figure 32: (a) Adsorption of Cellulose on the Surface of rGO by Hydrogen Bonds

(b) Methods for manufacturing a 3D rGO/Cellulose structure.

Furthermore, 3D porous structures with varying ratios of reduced graphene oxide (rGO) to cellulose were fabricated using the solution mixing method (Figure 32B). Graphene oxide (GO) is dispersible in water and certain organic solvents, facilitating its interaction via hydrogen bonds and shear forces to form an rGO-cellulose hydrogel. The dispersion in water and stability of rGO/cellulose films were subsequently investigated across different concentrations of rGO. Photographs depicting the rGO (x) / cellulose composites (x = 0, 0.1, 0.5, 1, 2, 5, and 10) after 8 hours of grinding are illustrated in Figure 33.

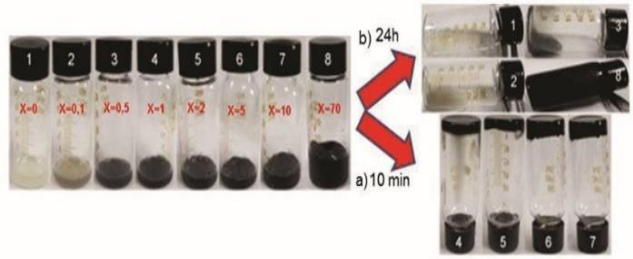

Figure 33: Photos of rGO(x)/Cellulose (100) Composites in water a) 10 Min After Synthesis and b) 24h after Synthesis (x = % weight / Cellulse)

As the content of reduced graphene oxide (rGO) increases, the synthesized composites darken. Moreover, all mixtures exhibit homogeneity, indicating uniform dispersion of rGO sheets within the composites. The viscosity of the composites rises with increasing rGO content due to hydrogen bond interactions between the hydroxyl groups of cellulose and residual oxygen groups on the rGO sheets.

The gelation of rGO(x) / Cellulose (100) (% by weight) mixtures with x = 1, 2, 5, and 10 occurs within 10 minutes (Figure IV.2a), whereas mixtures with x = 0, 0.1, and 0.5 do not gel easily (Figure IV.2b). However, an exception was noted for the rGO (70) / cellulose (100) composite, which only forms a semi-gelled state (Figure IV.2b8). This phenomenon is attributed to an excess of hydrazine in the mixture. The surplus hydrazine alters the ionic strength and promotes hydrogen bond-like interactions within the composite. The coagulating effect of cellulose retains rGO sheets in 3D structures.

These 3D porous structures of rGO composites/cellulose exhibit potential applications in the field of supercapacitors. Similarly, Zhang et al. synthesized graphene- and cellulose-based nanocomposite films in a DMAC/LiCl solution. The preparation of films through chemical modification of GO surfaces with cellulose was also investigated by Peng et al. using an ionic liquid solution (1-Butyl-3-methylimidazolium chloride ([Bmim]Cl)) (Figure 34).

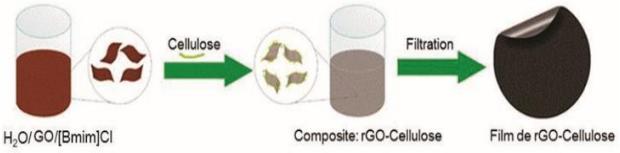

Figure 34: Chemical Modification of the Surface of GO by Cellulose in a Solution of Ionic Liquid

This chemical modification was characterized by UV-visible spectroscopy, IR spectroscopy, X-ray diffraction and Raman spectroscopy (Figure.35).

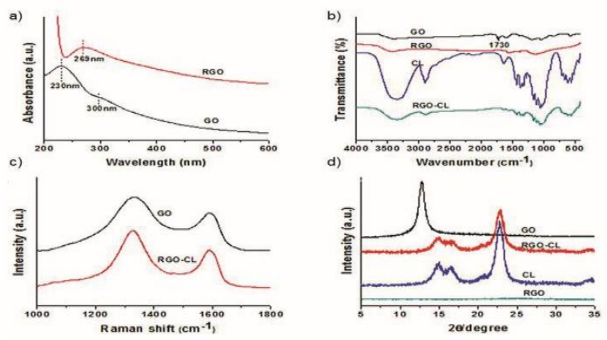

Figure 35: Analysis a) UV-Visible, b) IR, c) Raman Spectroscopy and d) X-ray diffraction of the Various Samples

UV-Visible analysis (Figure 35a) reveals that graphene oxide (GO) exhibits a characteristic peak at 231 nm, corresponding to the π-π* transitions of carbon-carbon bonds, alongside a shoulder at approximately 300 nm attributed to n-π* transitions of carboxyl bonds. Upon reduction, the peak at 231 nm redshifts to 269 nm, accompanied by the disappearance of the 300 nm absorption peak, indicating the restoration of electronic conjugation in reduced graphene oxide (rGO).

Infrared (IR) analysis (Figure 35b) shows decreased intensities of vibration bands from C-O at 1730 cm-1, and C-O (epoxy) and (alkoxy) vibration bands at 1220 cm-1 and 1058 cm-1, respectively, in the rGO spectrum, indicative of GO reduction. The IR spectrum of cellulose-grafted rGO closely resembles that of pristine cellulose, confirming the presence of cellulose on rGO nanosheets. Furthermore, restoration of the sp2 structure in rGO was confirmed by Raman spectroscopy. The Raman spectrum of GO exhibits prominent G and D bands at 1591 cm-1 and 1331 cm-1, respectively, which are also observed in the cellulose-functionalized rGO spectrum (rGO-CL). Notably, the ratio of D/G band intensities increased significantly from 1.32 to 1.53, indicating chemical modification of the rGO sheets.

X-ray analysis (Figure 35d) shows a characteristic diffraction peak of GO at 11.9° with an interlayer distance of 0.74 nm, which disappears in the rGO-CL and rGO spectra. Additionally, diffraction peaks appear at 15.1°, 16.8°, and 22.5° corresponding to the crystalline phase of cellulose, confirming cellulose adsorption onto GO.

xxiii. Covalent Approach

Hydroxyl groups on cellulose were utilized for functionalization through esterification reactions. Moreover, it was demonstrated that cellulose can be directly grafted onto graphene oxide (GO) or carbon nanotubes (CNTs) via covalent bonding, specifically through esterification reactions between the carboxylic acid groups of GO and the hydroxyl groups of cellulose. The resulting composite was employed in the fabrication of electroactive paper, with subsequent investigation into its mechanical properties and performance (Figure 36).

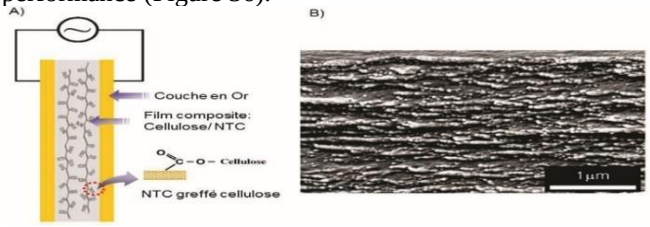

Figure 36: (a) Manufacture of Electronic Paper based on Cellulose Grafted CNT, (b) SEM Plate of the Cellulose/CNT Composite

Recently, numerous researchers have focused on chlorinating graphite oxide using thionyl chloride (SOCl2) to facilitate its chemical modification with polysaccharides. For instance, they functionalized "GO-Cl" with chitosan oligosaccharide lactate (LMC) and hydroxypropyl cellulose (HPC) (Figure 37).

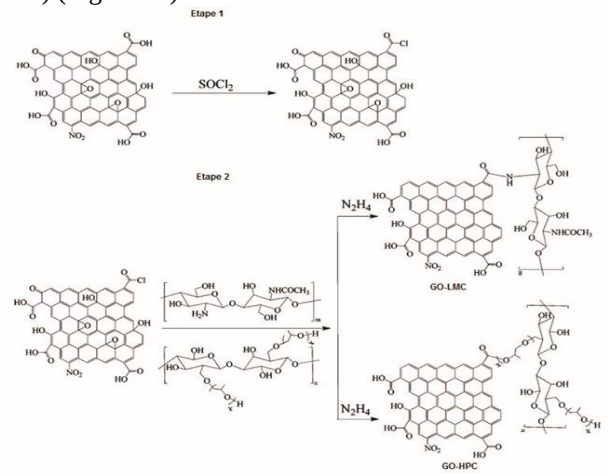

Figure 37: Chlorination of Oxidized Graphite with Thionyl Chloride Followed by Chemical

Functionalisation with polysaccharides. The amounts of HPC and CML grafted onto graphene were estimated by ATG (Figure 38).

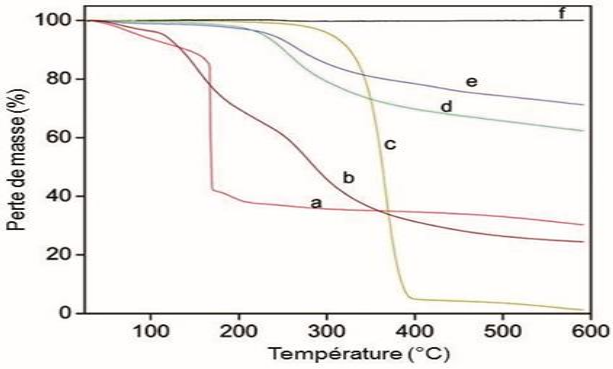

Figure 38: ATG Thermogram a) GO, b) Chitosan (LMC), c) Cellulose (HPC), d) GOLMC, e) GO-HPC and f) Graphite

The thermograms indicate distinct decomposition profiles for GO-HPC and GO-LMC compared to polysaccharides, graphite, and GO. Hydroxypropyl cellulose (HPC) degrades sharply at 342°C with a significant weight loss of 96% before reaching 400°C, while the degradation of GO-HPC initiates at approximately 228°C with a loss of about 30% up to 340°C, attributed to the decomposition of grafted HPC on GO. Chitosan oligosaccharide lactate (LMC) degrades around 123°C with an 85% weight loss and leaves a 20% residue at 600°C. In contrast, GO-LMC shows initial degradation around 210°C with a 20% weight loss, followed by a more substantial loss at 392°C due to the decomposition of grafted LMC chains on GO. Overall, based on the thermograms, it is inferred that GO-HPC and GO-LMC contain approximately 30% and 20% by weight of polysaccharides, corresponding to grafting densities of 0.033 mmol/g for cellulose and 0.048 mmol/g for chitosan, respectively.

xxiv. Grafting of Cellulose onto Oxidized Graphite in the Presence of Coupling Agent

To increase the amount of the polymer grafted on the substrate as well as to increase the finity of the GO with the polymer matrix, the idea is first to graftmolecules on the GO which will then serve as the anchoring site for cellulose (Figure.39).

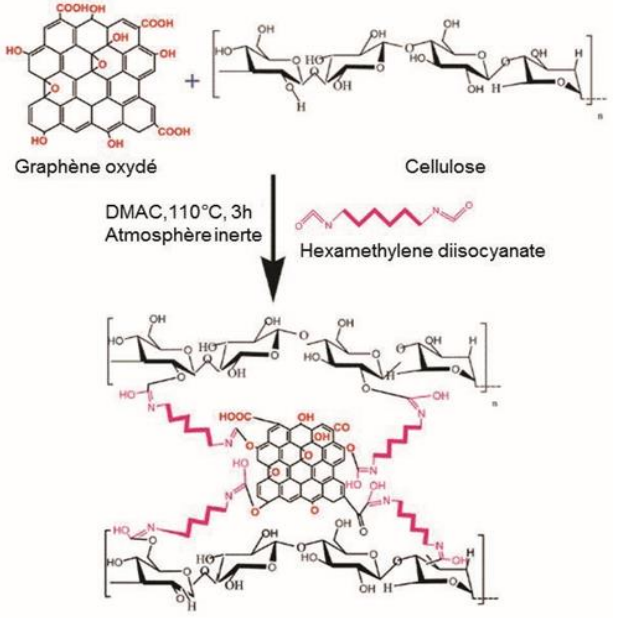

Figure 39: Chemical Modification of the Surface of GO by Cellulose in the Presence Hexamethylene Diisocyanate

Cellulose was grafted onto oxidized graphene using hexamethylene diisocyanate (Figure 39) and isophorone diisocyanate (Figure IV.10), achieving a grafting density of approximately 0.022 mmol/g depending on the molecular weight of the cellulose used. The authors prepared various nanocomposites of graphene oxide grafted with cellulose (CFG) for applications in energy storage and electronics. They demonstrated that these CFG nanocomposites exhibit ferroelectric behavior associated with integrated polarization that is commutative and temperature-dependent. The grafting process was characterized using various methods including X-ray diffraction (Figure 40).

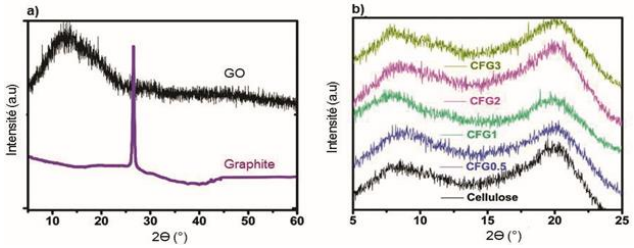

Figure 40: XRD Spectrum of a) Graphite and GO and b) CFG Nanocomposites

The diffraction peak of natural graphite at approximately 2Θ = 26.521° corresponds to an interlayer distance of 3.354 Å (Figure 40a). In the case of graphene oxide (GO), the peak indicates an interlayer distance of 8.0854 Å (Figure 40a). Figure I.8b provides insights into the crystal structure of nanocomposites and the dispersion of GO in cellulose. The broad diffraction peak at 19° suggests the partially crystalline nature of cellulose. However, the X-ray diffraction (XRD) spectra of all graphene oxide grafted cellulose (CFG) nanocomposites resemble that of cellulose, indicating efficient dispersion of GO within the cellulose matrix. Moreover, the GO peak is absent in the XRD spectra of CFG nanocomposites, confirming the exfoliation of GO nanosheets in the cellulose matrix.

Cellulose was grafted onto oxidized graphene in the presence of isophorone diisocyanate (Figure 41). This chemical modification enhances the development of proximity sensors with improved response speed and sensitivity.

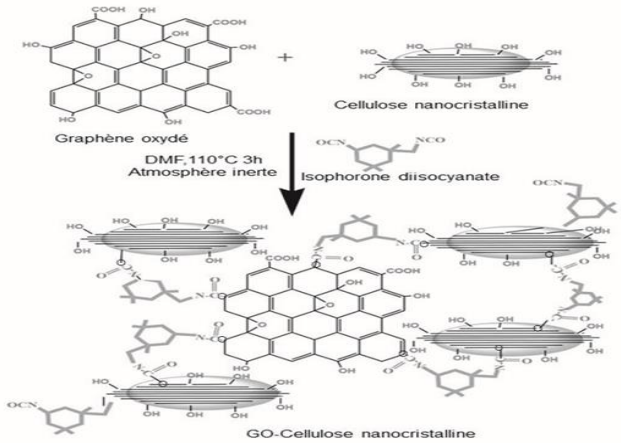

Figure 41: Chemical Modification of the Surface of GO by Isophorone Diisocyanate and Cellulose

The morphology of cellulose, graphene oxide (GO), and graphene oxide-cellulose nanocrystals (GO-CNC) was characterized using transmission electron microscopy (TEM). In Figure 42a, synthesized GO exhibits a flake structure and transparency. Figure 42b shows the starting cellulose with rod-shaped cellulose nanocrystals (CNCs) ranging from 100 to 300 nm in length. The nanocrystalline cellulose forms a dense network due to intermolecular interactions.

In the case of the GO-CNC sample (Figure 42c), the structure appears highly crosslinked due to the reaction between the hydroxyl groups of CNC and the isocyanate groups of Isophorone diisocyanate (IPDI) at the edges of the GO sheets. The GO nanolayers are observed stacked into thicker flakes, with GO monolayers encapsulated by CNC on the upper surface of the sample. At higher magnification (Figure 42d), the CNC network on the GO sheets is visible as white dots with a circular shape on the surface.

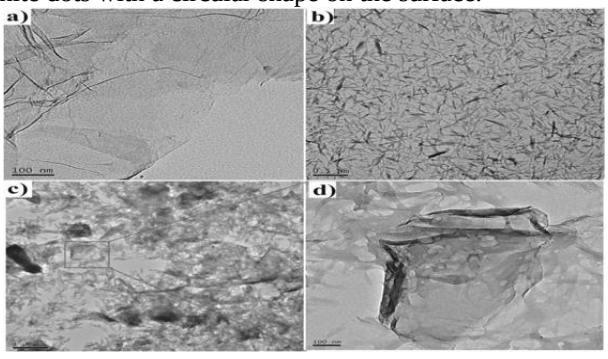

Figure 42: TEM images of a) GO, (b) CNC, (c) and (d) GO-CNC

This type ofgrafting makes it possible to envisage different applications in the field of the manufacture of chemical sensors or supercapacitors.

xxv. Grafting of Chitosan onto Oxidized Graphite

Graphene and chitosan-based nanocomposites find extensive applications in fields such as electrochemistry and biomaterials. Comparatively, grafting chitosan onto graphitic substrates is more straightforward than cellulose due to its solubility in dilute acetic acid. Separation of non-grafted chains can be easily achieved by centrifugation following the functionalization of graphene oxide (GO) with chitosan. This functionalization involves the formation of an amide linkage between the amine groups of chitosan and the carboxylic acid groups present on the edges of each GO sheet. Researchers demonstrated enhanced reinforcement of graphene-based nanocomposites through chemical functionalization of chitosan on the edges of GO sheets (Figure 43).

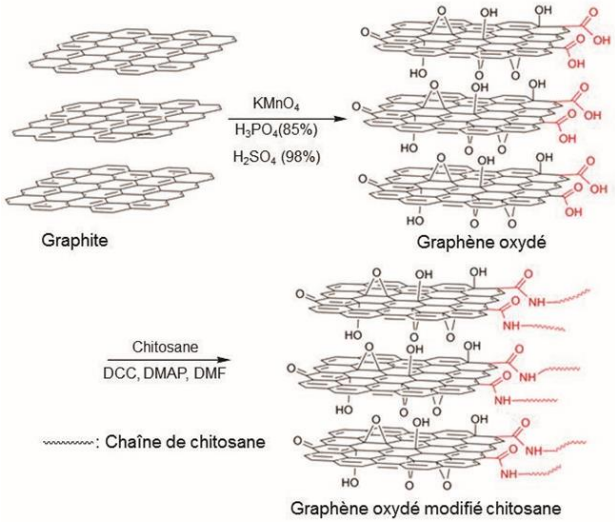

Figure 43: Direct Grafting of Chitosan onto the GO Substrate

They demonstrated that the tensile strength of the chitosan film increased from 32.7 to 82.0 MPa after grafting onto GO, with a grafting rate of 20%, as determined by thermogravimetric analysis (TGA) between 300 and 550 °C. In contrast, the tensile strength of the film derived from a GO/chitosan mixture containing 0.25% GO and 2.25% chitosan was 43.8 MPa (Figure 44).

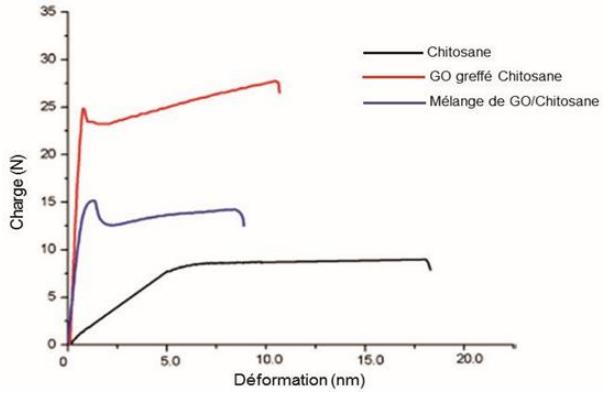

Figure 44: Tensile Behavior of Chitosan and GO Films

In addition, the addition of GO decreases the elongation at the breaking point . This could be attributed to the interaction between GO and the polymer matrix, which limits the regular motion of chitosan chains. The quantitative and qualitative analyses of this grafting are presented in the figure.45.

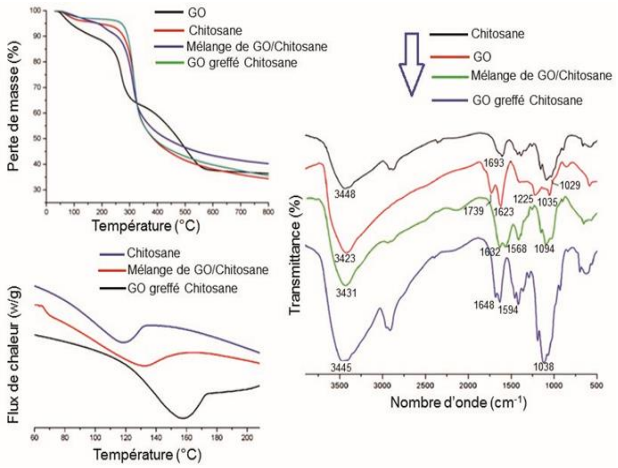

Figure 45: Thermograms (A) ATG and (B) DSC of Chitosan Transplanted GO and (C) Infrared Spectrum of Chitosan Transplanted GO

The thermal properties of graphene- and chitosan-based composite films were analyzed using thermogravimetric analysis (TGA) and differential scanning calorimetry (DSC). TGA results (Figure 45A) indicated that the initial graphene oxide (GO) powder exhibited thermal instability, whereas the GO-chitosan composite demonstrated improved thermal stability. A minor weight loss below 150°C was observed in the GO-chitosan film, attributed to the desorption of physisorbed water. No significant weight loss was noted up to 300°C, followed by major decomposition around 300°C, consistent with the degradation temperature of chitosan (Figure 45A). The grafting density of chitosan on GO was calculated as 3.75 × 10^-4 mmol/g.

Furthermore, the glass transition temperature (Tg) was observed at 118-119°C for chitosan alone, 132°C for the GO/chitosan mixture, and 158°C for the chitosan-grafted GO composite. These findings suggest decreased mobility of chitosan chains post-grafting, influencing thermal behavior.

In a separate study, chitosan was grafted onto GO surfaces using N-hydroxysuccinimide (NHS) and 1-ethyl-3-(3-dimethylaminopropyl) carbodiimide (EDC) to enhance the reactivity of carboxylic acid groups located on the GO edges (Figure 46 depicts the functionalization strategy).

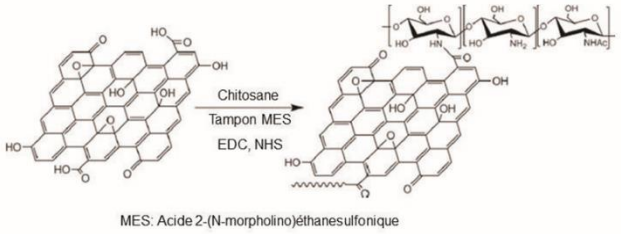

Figure 46: Functionalization of GO by Chitosan in the Presence of NHS and EDC Reagents

EDC was employed as an activator for carboxylic acid groups to facilitate the formation of an amide bond between graphene oxide (GO) and chitosan, leading to the formation of an intermediate that was subsequently stabilized by NHS addition. Additionally, a low molar mass (Mn = 3000 g/mol) was chosen to prevent cross-linking phenomena.

This functionalization was confirmed using ^1H NMR in D2O/DCl and FT-IR spectroscopy. Quantitative analysis via thermogravimetry (TGA) indicated that GO was functionalized with chitosan chains, resulting in a weight percentage of 64%, corresponding to a grafting density of 0.21 mmol/g (Figure 47).

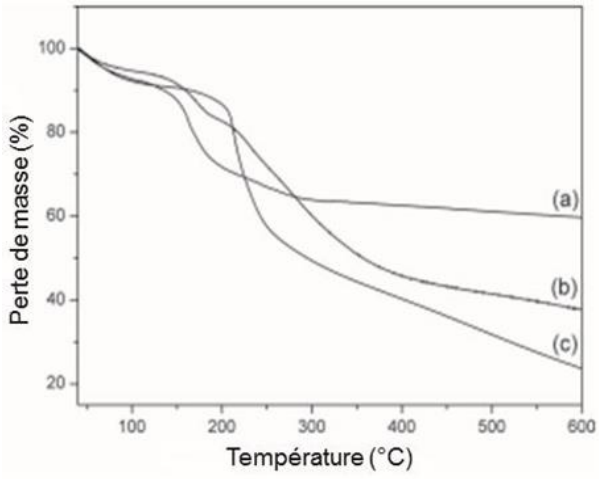

Figure 47: ATG curves of a) GO, b) GO-Chitosan and C) Chitosan (10°C/min Below Nitrogen)

Most recently, S. Sayyar also used lactic acid, N-hydroxysuccinimide (NHS) and 1-ethyl-3-(3-dimethylaminopropyl)carbodiimide (EDC) to perform chemical functionalization of GO with chitosan (Figure 48).

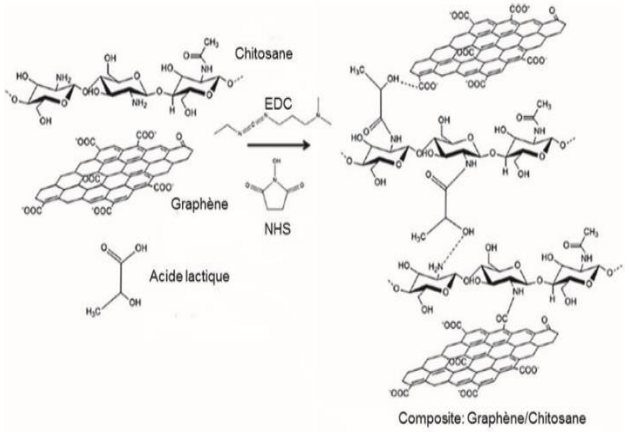

Figure 48: Functionalization of GO with Chitosan in the Presence of Lactiq Acidand NHS and EDC Reagents

Lactic acid facilitates the bridging of chitosan chains through hydrogen bonds. Alternatively, chitosan can be directly grafted onto graphene oxide (GO) through the formation of amide bonds, achieving a grafting density of 3.10^-4 mmol/g. A mechanism illustrating the formation of amide bonds between amine and carboxylic acid groups using NHS and EDC is presented in Figure 49.

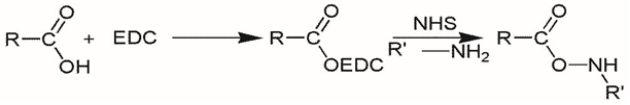

Figure 49: Formation of Anamicide Function between a Carboxylic Acid Function and a amine Function Activated by NHS and EDC Reagents

Their study demonstrated that a controllable increase in the electrical conductivity of the prepared nanocomposite was possible by increasing the amount of GO in this material (Figure.50).

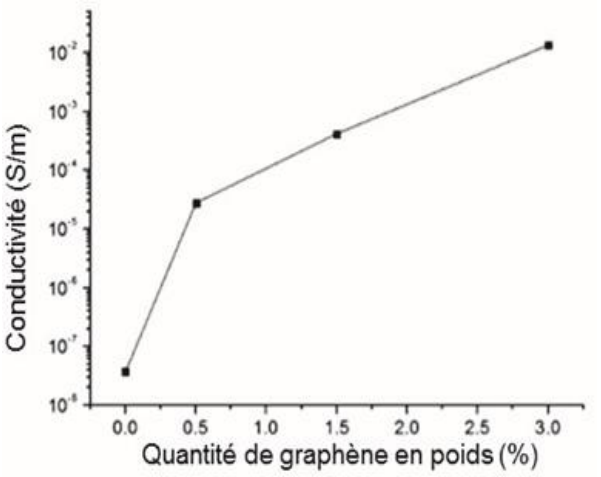

Figure 50: Measurement of the Electrical Conductivity of the film as a Function of the Percentage in Graphene Weight

The incorporation of graphene enhances the electrical conductivity of the GO-chitosan film. Pure chitosan typically exhibits a conductivity of approximately 10^-8 S.m^-1. However, the conductivity of the composite significantly increases to 10^-5 S.m^-1 with a graphene content of 0.5% by weight. The maximum conductivity reaches approximately 1.4 × 10^-2 S.m^-1 with a graphene content of 3% by weight, beyond which the conductivity stabilizes.

For catalytic purposes in the reduction of 4-Nitrophenol to 4-Aminophenol, Rajesh grafted chitosan onto GO using the standard method of chlorinating COOH groups located at the edges of the GO sheets, followed by adsorption of gold nanoparticles onto the composite (Figure 51a).

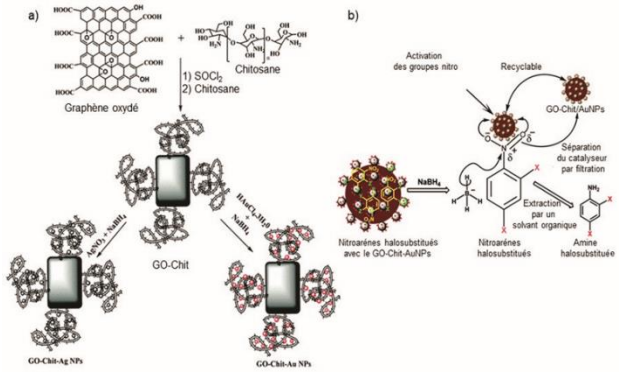

Figure 51: a) Functionalization of GO by Chitosan and Adsorption of Gold and Silver Nanoparticles, b) Schemaa of the Mechanism of Catalytic Reduction of Nitroarenes by Metal Nanoparticles Adsorbed on GO-Chitosan

These surface-adsorbed nanoparticles serve as catalysts for the reduction reaction of 4-nitrophenol to 4-aminophenol in the presence of sodium tetrahydruroborate (NaBH4) (Figure 51b). Borohydride ions (BH4-) interact with the nanoparticles' surface, facilitating the transfer of hydrogen ions to the reaction site. Concurrently, nitroarene molecules are adsorbed onto the nanoparticle surface, and both adsorption and desorption processes are reversible. The final step in this catalytic cycle involves the desorption of the formed aminophenol, after which the catalyst can be easily removed by filtration.

The extent of chitosan grafting onto graphene oxide (GO) was quantified using thermogravimetric analysis (TGA), specifically by measuring the mass loss between 200 and 800°C (Figure 52).

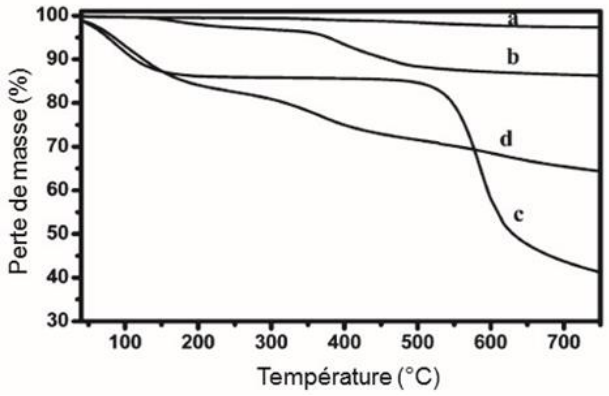

Figure 52: ATG Thermogram of (a) Pure Graphite, (b) GO, (c) Chitosan and (d) GO Chitosan

The thermogram of GO-Chitosan (Figure 52d) indicates a weight loss of approximately 16% below 400°C, attributed to the decomposition of chitosan glucopyranose chains and residual functional groups on the graphene oxide (GO) sheets. The calculated grafting density is 0.05 mmol/g.

Subsequently, this functionalization process involved the adsorption of gold nanoparticles (AuNPs), which was characterized using transmission electron microscopy (TEM) (Figure 53).

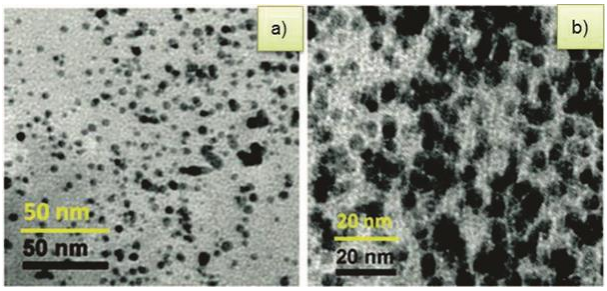

Figure 53: TEM Images of GO-Chitosan Doped AuNPs

Figure 53a depicts a transmission electron microscopy (TEM) image of GO-Chitosan decorated with gold nanoparticles (AuNPs), each with a diameter of approximately 20 nm. Furthermore, Figure 53b illustrates a uniform dispersion of these AuNPs.

V. CONCLUSION

The literature review provided a comprehensive overview of the fundamental studies and applications related to graphene. It discussed the different allotropic forms of graphite and the various techniques used to prepare graphene from graphite. Additionally, the review covered the methods of functionalizing graphite and graphene oxide (GO) through common organic chemistry reactions.

The review then focused on the mechanical, thermal, and diverse industrial, pharmaceutical, and biomedical applications of graphene-based materials. Furthermore, it explored polysaccharides, particularly cellulose and chitosan, and their use in the development of biocomposites, including their preparation, characterization, properties, and applications in different fields.

Lastly, the review presented the different methods of grafting polysaccharide chains (cellulose and chitosan) onto the surface of GO. The review highlighted that the covalent functionalization of cellulose directly on GO by the chlorination of COOH functions located on the edges of GO sheets resulted in a grafting percentage of 30 wt%, corresponding to a grafting density of 0.033 mmol/g. In contrast, the grafting method in the presence of a coupling agent yielded a grafting percentage of 20 wt%, or a grafting density of 0.022 mmol/g. For chitosan, the chemical functionalization directly on GO in the presence of EDC and NHS as activators of amide bond formation gave a grafting percentage of 64 wt%, which corresponds to a grafting density of 0.21 mmol/g. The review discussed that the difference in grafting density depends on various factors, such as the molar mass of the polysaccharides and the grafting method used.

DECLARATION STATEMENT

I must verify the accuracy of the following information as the article's author.

- **Conflicts of Interest/Competing Interests:** Based on my understanding, this article has no conflicts of interest.
- **Funding Support:** This article has not been sponsored or funded by any organization or agency. The independence of this research is a crucial factor in affirming its impartiality, as it has been conducted without any external sway.
- **Ethical Approval and Consent to Participate:** The data provided in this article is exempt from the requirement for ethical approval or participant consent.
- **Data Access Statement and Material Availability:** The adequate resources of this article are publicly accessible.
- **Authors Contributions:** The authorship of this article is contributed solely.

REFERENCES

1. Machkour A, Thallaj NK, Benhamou L, Lachkar M, Mandon D.Chemistry. 2006 Aug 25;12(25):6660-8.P 6660-6661-6662-6663. https://doi.org/10.1002/chem.200600276
2. Thallaj, N., Machkour, A., Mandon, D., Welter, R., New. J. Chem., 2005, 29, 1555 – 1558. https://doi.org/10.1039/b512108f
3. Thallaj NK, Rotthaus O, Benhamou L, Humbert N, Elhabiri M, Lachkar M, Welter R, Albrecht-Gary AM, Mandon D. Chemistry. 2008;14(22):6742-53.P6745-6746-6747. https://doi.org/10.1002/chem.200701967
4. Wane A, Thallaj NK, Mandon D. Chemistry. 2009 Oct 12;15(40):10593-602. P10594-10595-10595. https://doi.org/10.1002/chem.200901350
5. Thallaj NK, Orain PY, Thibon A, Sandroni M, Welter R, Mandon D. Inorg Chem. 2014 Aug 4;53(15):7824-36. P7826-7827-7828. https://doi.org/10.1021/ic500096h
6. N. K. Thallaj, J. Przybilla, R. Welter and D. Mandon, J. Am. Chem. Soc. 2008, 130, 2414-2415. https://doi.org/10.1021/ja710560g
7. N. K. Thallaj, D. Mandon and K. A. White, Eur. J. of Inorg. Chem., 2007, 44–47. https://doi.org/10.1002/ejic.200600789
8. Thallaj, N.; International journal of applied chemistry and biological sciences 2021, 2 (4), 65-77.
9. Thallaj, N.; Indian Journal of Advanced Chemistry (IJAC)2021, 1 (2), . https://doi.org/10.54105/ijac.D2015.102222
10. Thallaj, N.; International Journal of Research Publication and Reviews (IJRPR)2021, 2, 10, 951-959

11. L. Labban, N. Thallaj, Z. Malek; International Journal of Medical Studies, 2020, 5, No 12, 23-36. https://doi.org/10.36648/1989-5216.12.3.309
12. L. Labban, M. Kudsi, Z. Malek, N. Thallaj; Advances in Medical, Dental and Health Sciences, 2020,3, 3,45-48. https://doi.org/10.5530/amdhs.2020.3.11
13. L. Labban, N. Thallaj, M. Al Masri; Journal of Advanced Research in Food Science and Nutrition, 2020,3,1,34-41. https://doi.org/10.11648/j.wjfst.20190304.11
14. L. labban; N. thallaj; A. labban; archives of medicine, 2020, 12, 2:8, 1-5. https://doi.org/10.36648/1989-5216.12.3.309
15. L. labban; N. thallaj; international journal of herbal medicine,2020, 8, 2, 33-37.
16. L. Labban, N. Thallaj, Z. Malek; Journal of Medical Research and Health Sciences, 2019, 2, 11, 784-787.
17. L. labban N. Thallaj; acta scientific nutritional health, 2019, 3,10, 7-12. https://doi.org/10.31080/ASNH.2019.03.0435
18. Malek, Z.S.; Sage D.; Pevet, P.; Raison, S.; Endocrinology 2007, 148 (11), 5165-5173. https://doi.org/10.1210/en.2007-0526
19. Malek, Z.S.; Dardente, H.; Pevet, P.; Raison, S.; European Journal of Neuroscience 2005, 22 (4), 895-901. https://doi.org/10.1111/j.1460-9568.2005.04264.x
20. Malek, Z.S.; Pevet, P.; Raison, S.; Neuroscience 2004, 125 (3), 749-758. https://doi.org/10.1016/j.neuroscience.2004.01.031
21. Malek, Z.S.; Labban, L.; The International Journal of Neuroscience, 2020, 1-7.
22. Malek, Z.S.; Labban, L.; European Journal of Pharmaceutical and Medical Research 2019, 6 (11), 527-532.
23. Malek, Z.S.; Journal of AlBaath University 2018, 40 (4), 39-62.
24. Malek, Z.S.; Tishreen University Journal for Research and Scientific Studies, 2018, 40.
25. ZS Malek, LM Labban; International Journal of Neuroscience, 2021,131 (12), 1155-1161. https://doi.org/10.1080/00207454.2020.1782903
26. ZS Malek, LM Labban; Journal of current research in physiology and pharmacology, 2020, 4, (1),1-5.
27. L.M. Labban, M. M. Alshishkli, A. Alkhalaf, Z. Malek; J. Adv. Res. Dent. Oral Health, 2017, 2(3&4), 1-4.
28. L Labban, ZS Malek, Open Access Library Journal, 2018, 5 (07), 1-11. https://doi.org/10.4236/oalib.1104654
29. L Labban, ZS Malek, Ann Food Nutr Res J, 2019,1 ,1
30. Labban, L. and N. Thallaj, 2019. Acta Scient. Nutr. Health, 3: 7-12. https://doi.org/10.36648/1989-5216.12.3.309
31. Y. alhomush, Z. malek, A. Abboud, N.Thallaj, Research Journal of Pharmacy and Technology, 2022, 15, 10.
32. Thallaj, Nasser. "تخليق مشتقات 1، 3، 4-أوكسديازول، ثيازوليدين بمساعدة المايكرويف." Tishreen University Journal-Medical Sciences Series44.1 (2022): 59-77.
33. N.Thallaj, Tishreen university journal,2022,44,2, 87-105.
34. N.Thallaj. Indian journal of advanced chemistry, 1, 3, 2022. 10-14.
35. Thallaj, Nasser. "Characterization of charge heterogeneity of antibody-drug conjugate by anion-exchange chromatofocusing." Tishreen University Journal-Medical Sciences Series 44.6 (2022): 21-29.
36. A.Abbood, Z.Malek, N.Thallaj. 2022 15, 11, 4935-4939. Research Journal of Pharmacy and Technology. https://doi.org/10.52711/0974-360X.2022.00829
37. L. Alallan, Z.malek, (2023). 45,(1) 73-81. Tishreen University Journal-Medical Sciences Series.
38. Thallaj, Nasser, and Mays Khazem. "Studying the efficacy of the plant extract of Tetracera scandens as an antidiabetic treatment." Tishreen University Journal-Medical Sciences Series 45.1 (2023): 33-44.
39. N.Thallaj. International Journal of Advanced Pharmaceutical Sciences and Research (IJAPSR) 2022. 2, 3,1-28 https://doi.org/10.54105/ijapsr.C4018.042322
40. N.Thallaj. International Journal of Advanced Pharmaceutical Sciences and Research (IJAPSR) 2022. 2, 4,1-15. https://doi.org/10.54105/ijapsr.C4016.062422
41. N.Thallaj. International Journal of Advanced Pharmaceutical Sciences and Research (IJAPSR) 2022. 2, 6,1-12. https://doi.org/10.54105/ijapsr.C4015.102622
42. Thallaj, Nasser. "Review of a Few Selected Examples of Intermolecular Dioxygenases Involving Molecular Oxygen and Non-Heme Iron Proteins." Int. J. Adv. Parmacutical Sci. Res.(IJAPSR) 3 (2023): 1-18. https://doi.org/10.54105/ijapsr.C4011.023223
43. Thallaj, Nasser, and Ayat Abbood. "مقارنة بين مرتسمات الكروماتوغرافيا icIEFالبؤرية و لمغايرات الشحنة لأضداد وحيدة النسيلة عارية ومرتبطة مع دواء." Tishreen University Journal-Medical Sciences Series 45.2 (2023): 47-57.
44. Dayoub, Leen, Yanal Alkuddsi, and Nasser Thallaj. "Investigating the interaction between some of Bipolaris sorokiniana's toxins and the Gα Subunit of the Wheat G-Protein using bioinformatics tools." University of Thi-Qar Journal of agricultural research 12.1 2023. https://doi.org/10.54174/utjagr.v12i1.253
45. Thallaj, N; agha, M. I ,H;, nattouf; A.H; katib, CH; karaali, A; Moustapha, A; Labban L;open access library journal, 2020,7,5,1-21.. https://doi.org/10.4236/oalib.1106302
46. N.Thallaj. Indian journal of advanced chemistry, 1, 3, 2022. 10-14.
47. N.Thallaj.Xi'an ShiyouDaxueXuebao (ZiranKexue Ban)/ Journal of Xi'an Shiyou University, Natural Sciences Edition.2022.65, 06. 289-301.
48. N.Thallaj.Xi'an ShiyouDaxueXuebao (ZiranKexue Ban)/ Journal of Xi'an Shiyou University, Natural Sciences Edition.2022.65, 06. 313-328.
49. Z. MALEK, A. ABBOOD, N.THALLAJ. Xi'an ShiyouDaxueXuebao (ZiranKexue Ban)/ Journal of Xi'an Shiyou University, Natural Sciences Edition.2022.65, 06. 302-312.
50. N.Thallaj. 2022. 65, 7, 169-184. Xi'an Shiyou Daxue Xuebao (Ziran Kexue Ban)/Journal of Xi'an Shiyou University, Natural Sciences Edition.
51. N.Thallaj. 2022. 65, 7, 110-142. Xi'an Shiyou Daxue Xuebao (Ziran Kexue Ban)/Journal of Xi'an Shiyou University, Natural Sciences Edition.
52. N Thallaj, (2023). 44,(6),21-29. Tishreen University Journal-Medical Sciences Series.
53. N.Thallaj. International Journal of Advanced Pharmaceutical Sciences and Research (IJAPSR) 2022. 2, 6,1-12. https://doi.org/10.54105/ijapsr.C4015.102622
54. N.Thallaj. International Journal of Advanced Pharmaceutical Sciences and Research (IJAPSR) 2023. 3, 3,1-10.
55. N.Thallaj. International Journal of Advanced Pharmaceutical Sciences and Research (IJAPSR) 2024. 4, 1,32-52.
56. N.Thallaj. International Journal of Advanced Pharmaceutical Sciences and Research (IJAPSR) 2024. 4, 3,6-19.
57. N.Thallaj. International Journal of Advanced Pharmaceutical Sciences and Research (IJAPSR) 2024.4, 4,7-21. https://doi.org/10.54105/ijapsr.D4042.04040624
58. Besherb S, Alallan L, Hassan Agha MA, AIshamas I, Thallaj N. Influence of soil salinity on the chemical composition of essential oil of Rosmarinus Officinalis in Syria, Research J. Pharm. and Tech. 2024; 17(4). https://doi.org/10.52711/0974-360X.2024.00358
59. Isbera M, Abbood A, Ibrahim W. Weight and Content Uniformity of Warfarin Sodium Half Tablets. Research J. Pharm. and Tech. 2016; 9(3):215-218. doi: 10.5958/0974-360X.2016.00039.1 https://doi.org/10.5958/0974-360X.2016.00039.1
60. Abbood A, Layka R. Weight and content uniformity Study of captopril half-tablets. Research J. Pharm. and Tech. 2017;10(6):1621-1626. doi: 10.5958/0974-360X.2017.00285.2. https://doi.org/10.5958/0974-360X.2017.00285.2

AUTHOR PROFILE

Porf. Dr. Nasser Thallaj, 2020- presente time: professor in the biomedical Science program.
2020- Present time: *Assistant professor* position. Faculty of pharma *alrashed university*, Damascus, syria
From 15 june 2019 – 31 July 2020: President Of *AlJazeera University*, Damascus, Syria.
From Abril 1st 2019 – 15jun: vice president for scientific affairs and Dean of Faculty of pharmacy AlJazeera University, Damascus, Syria.
From October 1st 2018-15 march 2020: Dean of Faculty of pharmacy *AlJazeera University*, Damascus, Syria.
2017-31 July2020: *Assistant professor* position. Faculty of pharmacy, *AlJazeera University*, Damascus, Syria
- 2015-2017: *Assistant professor* position. Faculty of pharmacy, *Syrian Private University*, Damascus, Syria
- 2015- 2016: Consultant in Ugarit Education Group: foundation of *AlManara University.*
- 2014-2015: vice president for scientific affairs (in charge), *University of Kalamoon*, Dier Attieh, Syria.
- 2014-2015: In charge of higher education affairs, *University of Kalamoon*, Dier Attieh, Syria.
- 2012-2014: Dean of Faculty of applied Sciences, *University of Kalamoon*. Dier Attieh, Syria.

- 2010-2013: Head of Department of Chemistry. Faculty of applied Sciences, *University of Kalamoon*. Dier Attieh, Syria
-2008: *Assistant professor* position. Faculty of applied Sciences, *University of Kalamoon.* Dier Attieh, Syria
2007-2008: Post-Doctoral position. *Laboratory of NanoOrganic Chemistry, and Supramolecular Materials*, thesis title: *drug delivery system Department* of Chemistry. *University Notre Dame de la Paix*. Namur, Belgium.